ABSTRAK

JUDUL ABSTRAK

Oleh
Ahmad Izzuddin
NIM: 1908919

Abstrak merupakan penjelasan singkat dan padat tentang pekerjaan dan hasil penelitian TA, yang dituliskan secara teknis. Abstrak memiliki karakter tegas dan komprehensif, dan hanya dapat dituliskan setelah pekerjaan penelitian telah mencapai tahap tertentu, dan karenanya ada hasil penelitian yang dapat dilaporkan. Abstrak ditulis menjelang akhir penyelesaian penulisan buku TA.

Secara umum, abstrak memuat beberapa komponen penting, yaitu: konteks atau cakupan pekerjaan penelitian, tujuan penelitian, metodologi yang digunakan selama penelitian, hasil-hasil penting yang dapat ditambahkan dengan implikasinya, dan simpulan dari penelitian. Dengan demikian, suatu abstrak tidak dapat dituliskan apabila penelitian belum mencapai hasil tertentu, apalagi kalau penelitiannya pun belum dilakukan.

Panjang abstrak sebaiknya dicukupkan dalam satu halaman, termasuk kata kunci. Tiga kata kunci dipandang cukup, yang masing-masingnya memuat paduan kata utama, yang dapat merepresentasikan isi Abstrak. Halaman Abstrak tidak memuat informasi judul dan penulis, sehingga tidak secara langsung dapat digunakan sebagai lembaran Abstrak Sidang TA yang disediakan untuk hadirin, yang memerlukan tambahan (sekurangnya) dua informasi tersebut.

Kata kunci: Konsep Abstrak, Komponen Abstrak, Kata Kunci.

ABSTRACT

TITLE

by
Ahmad Izzuddin
NIM: 1908919

In general, Abstract is a translation of Abstrak. However, appropriate paraphrase may need some words or sentences whose meanings are close enough to those written in Abstrak.

Key words: Abstract Concepts, Abstract Components, Key Words.

PENGESAHAN

APPROXIMATING SOLUTIONS OF *PARTIAL DIFFERENTIAL EQUATIONS* WITH PSUEDOSPECTRAL METHODS AND *SUPPORT VECTOR MACHINE*

Oleh

Ahmad Izzuddin

NIM 1908919

Program studi Sarjana Fisika

Fakultas Matematika dan Ilmu Pengetahuan Alam

Institut Teknologi Bandung

Menyetujui

Bandung, December 26, 2024

Dosen Pembimbing,

Prof. Dr. Lala Septem Riza, M.T.

NIP. 197809262008121001

Tim Penguji:

1. Nama Penguji 1
2. Nama Penguji 2

PEDOMAN PENGGUNAAN
BUKU TUGAS AKHIR

Buku Tugas Akhir Sarjana ini tidak dipublikasikan, namun terdaftar dan tersedia di Perpustakaan Institut Teknologi Bandung. Buku ini dapat diakses umum, dengan ketentuan bahwa penulis memiliki hak cipta dengan mengikuti aturan HaKI yang berlaku di Institut Teknologi Bandung. Referensi kepustakaan diperkenankan dicatat, tetapi pengutipan atau peringkasan hanya dapat dilakukan seizin penulis, dan harus disertai dengan kebiasaan ilmiah untuk menyebutkan sumbernya.

Memperbanyak atau menerbitkan sebagian atau seluruh buku Tugas Akhir harus atas izin Program Studi Sarjana Fisika, Fakultas Matematika dan Ilmu Pengetahuan Alam, Institut Teknologi Bandung.

Tugas Akhir ini dipersembahkan untuk
Tuhan, Bangsa, dan Almamater

KATA PENGANTAR

Kata pengantar berperan sebagai gerbang masuk bagi pembaca dan mendapat sajian ringkas tentang hal-hal terkait paparan pada buku Tugas Akhir (TA). Sajian ini sejatinya merupakan pengenalan umum bagi pembaca tentang isi tulisan. Hal ini berbeda dengan abstrak yang mendeskripsikan pekerjaan dan hasil penelitian secara lebih teknis.

Kata pengantar merupakan wadah penulis untuk mengenalkan dan mempromosikan pekerjaan dan hasil penelitian dengan bahasa yang sederhana, sehingga pembaca tertarik untuk menelusuri lebih jauh dengan mencermati seluruh paparan pada buku TA. Ini salah satu tujuan kata pengantar. Contoh paragraf yang mengantar pembaca pada isi Buku TA: *Template* LaTeX diberikan berikut ini.

Menuliskan pekerjaan dan hasil penelitian TA dalam suatu laporan buku TA memerlukan panduan standar. Panduan ini dibuat dalam beberapa dokumen, yang salah satunya adalah Buku TA: *Template* LaTeX. Suatu template adalah cetakan yang siap dituang oleh curahan buah pikiran yang keluar dari pengalaman dalam melakukan pekerjaan penelitian dan hasil-hasilnya. Mencermati cetakan yang memberikan sejumlah contoh dapat memperlancar penulisan laporan tersebut menjadi suatu produk, yaitu buku TA.

Tujuan lain dari Kata Pengantar adalah memberi tempat untuk menyampaikan rasa syukur dan terima kasih kepada banyak pihak, misalnya keluarga, staf akademik, staf tenaga kependidikan, teman, individu atau komunitas pemberi dukungan dan inspirasi, dan institusi pendukung pendanaan seperti pemberi beasiswa atau dana penelitian, atau pendukung akses fasilitas.

Pengorbanan, kegigihan, dedikasi, dan penuh tanggung jawab dari para pahlawan pekerja medis dalam perawatan pasien terpapar Covid-19 telah memberi inspirasi melalui nilai-nilai kejuangan tanpa pamrih. Inspirasi inilah yang membangkitkan spirit pamungkas pada penyelesaian Buku TA: Template LaTeX *ini. Suatu inspirasi selalu bekerja dan mengena secara tidak langsung. Banyak berterima kasih atas inspirasi yang memantik spirit ini.*

Tidak ada sub bab/bagian pada Kata Pengantar, namun daftar rincian diperkenankan. Pada bagian indentitas akhir, seperti berikut ini, dituliskan nama mahasiswa dan NIM, bukan *penulis*, dan tidak perlu ditandatangani. Berikut adalah contoh penulisan rincian yang berisi ucapan terima kasih:

- Prof. Dr. Lala Septem Riza, M.T. dan Dr. Muhammad Nursalman, M.T. selaku dosen pembimbing tugas akhir.
- Jyesta, sebagai teman bimbingan yang selalu bersedia untuk diajak berdiskusi selama penelitian.
- Rekan-rekan Spectranova, ...

Bandung, December 26, 2024

Ahmad Izzuddin
1908919

Contents

DAFTAR NOTASI

Notasi	Arti
$F_{\mu\nu}$	Tensor Elektromagnetik
$R^{\mu}_{\ \alpha\nu\beta}$	Tensor Riemann
$\Gamma^{\rho}_{\mu\nu}$	Simbol Christoffel
$g_{\mu\nu}$	Tensor Metrik
A_{μ}	Medan Gauge
$R_{\mu\nu}$	Tensor Ricci
$\mathscr{L}$	Densitas Lagrangian
$\hbar$	Konstanta Planck Tereduksi
$\mathbb{R}$	Himpunan Bilangan Real

DAFTAR SINGKATAN

Notasi	**Arti**
FWHM	*Full width half maximum*
rms	*root mean square*
RFS	*Rotary forcespinning*
PVP	Polivinil pirolidon
SI	Satuan Internasional

List of Figures

List of Tables

CHAPTER I

INTRODUCTION

1.1 Background

Partial differential equations (PDE) are a common tool widely used in the modern scientific understanding and many engineering processes. This is because many systems can be described by the way they change and often this can be more intuitive. As an example, think of someone heating up a large frying pan on a gas stove. To describe how the pan heats up when the center is right above the burner, one can say that the center would heat up first followed by its surroundings. Eventually the pan would not heat up any further. Also notice that the edges of the pan would always be cooler than the center. However, once a more complex setup is introduced such as an uneven heat source or more complex materials with different heat rates of transferring heat it becomes much harder to describe how the pan heats up. A more useful way to describe the system is using the heat equation. For a temperature function $u(\mathbf{x},t)$ of spatial coordinates vector $\mathbf{x}$ and time t, the generalized heat equation is defined in equation (1.1).

$$\frac{\partial u}{\partial t} = \nabla \cdot (\alpha \nabla u) \tag{1.1}$$

The divergence operator $\nabla\cdot$ denotes sum of all first spatial derivatives. In three dimensions this is $\nabla\cdot = \frac{\partial\cdot}{\partial x_1} + \frac{\partial\cdot}{\partial x_2} + \frac{\partial\cdot}{\partial x_3}$. And the gradient operator ∇ is the vector of all first spatial derivatives which in three dimensions is $\nabla f = \begin{bmatrix} \frac{\partial f}{\partial x_1} & \frac{\partial f}{\partial x_2} & \frac{\partial f}{\partial x_3} \end{bmatrix}^\mathsf{T}$. This equation says that the rate at which the temperature changes in time $\frac{\partial u}{\partial t}$ is proportional to how different the differences in temperature of a spot in the pan with its surroundings $\nabla^2 u$ multiplied with thermal diffusivity parameter α. One example of an insight this gives is that given a homogeneous material (α is constant) and the stove outputs heat at a constant rate the temperature will no longer change for a particular point once the temperature difference is constant. In other words once the function $u(\mathbf{x},t)$ at some time $t > 0$ approaches a linear function in space, the temperature at all spots will no longer change in time. Mathematically this is because the time derivative is zero if the

second spatial derivatives are also zero. Intuitively this is because once the temperature distribution approaches linear, the current spot on the pan is outputting as much heat it is getting. This insight is an example of why PDEs are useful.

Many other fields in physics such as waves, quantum dynamics, fluid dynamics, elastics, and many more also define systems using PDEs. PDEs are also used outside the physical sciences. In Finance, the Black-Scholes-Merton or Black-Scholes equation models the dynamics of the financial market. In ecology, PDEs are used to model population growth which is useful for modelling location dependent carrying capacity. This is used to model species distribution which can help develop better conservation policies. In the social sciences, PDEs such as the cross-diffusion model is used to explore the evolution of the urban environment (Jin et al., 2023). Crowd dynamics is another field where researchers have found it useful to model using PDEs (Hughes, 2000; Mukherjee et al., 2015). These are used to model dynamics such as shock-waves, pathing, and crowd flow as a whole. There are a variety of applications, ranging from bird flocks, pedestrian crowds, to robotic swarms (Gong et al., 2023).

An increasingly critical use of PDEs is in Numerical weather prediction (NWP). The information weather forecasts provide is an integral part of modern life. Many sectors rely on timely and accurate weather forecasts. Individuals, day to day rely on forecasts for a range of different decisions ranging from activities they can do to personal safety from extreme weather. The weather also affects retail as consumer behavior change with whether it is rain or shine (Govind et al., 2020; Moon et al., 2018; J. Tian et al., 2018; X. Tian et al., 2021). Similarly, the types of transportation people use and operational decisions changes with the weather (Lepage & Morency, 2021; Nurmi et al., 2013). Another critical sector is agriculture, where extreme weather events and changes in climate threatens the food supply (Anwar et al., 2013; Cogato et al., 2019; Malhi et al., 2021). As the climate continues to warm and extreme weather events increase in frequency, the mitigation for these events become all the more important (*Climate Change 2022*, 2023). Because of this, forecasting is critical in making accurate decisions for policymakers and warnings of extreme weather events for civilians (Astitha & Nikolopoulos, 2023; Stott et al., 2016). A major challenge is the fact that observations of weather can be sparse in the sense that observations are localized and do not cover entire areas (Galkin et al., 2020; Monmonier, 1999; Wilby & Yu, 2013). This lack of spatially distributed meteorological information

hampers decision-making on areas to be prioritized and what to prioritize based on location. For example, weather stations can only observe their immediate surroundings. And they are for the most part stationary. Even more mobile observation platforms like satellites only show the portion of the surface the satellite can see at any one time such as in figure 1.1. While accumulating observations through more satellite passes is possible, this, however, means short-lived features may not be observed. As impoverished regions often are the most data sparse, the effect compounds on the fact that for impoverished regions, scarce resources need to be effectively and efficiently applied. To this end, numerical models are employed to model a more representative view by using known physics such as the compressible Euler equations and statistical models (Kwasniok, 2012; Mengaldo et al., 2019). The next step is in forecasting future weather which in itself is a challenge. The information this could provide is invaluable because it means planning for future weather is possible.

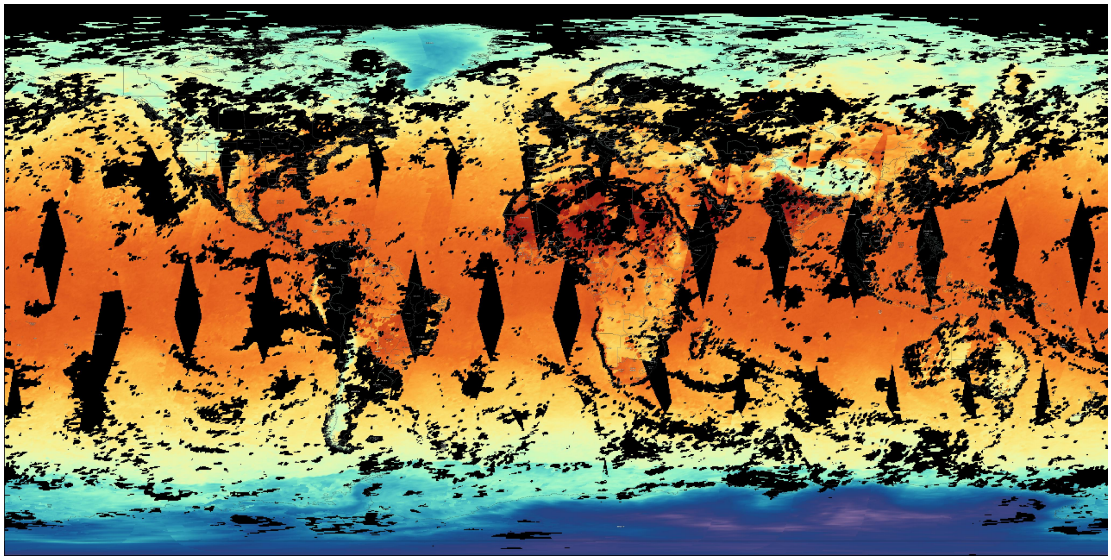

Figure 1.1: Daytime and nighttime surface air temperature from observations by the AIRS instrument onboard the NASA AQUA satellite. This shows observations recorded through a whole day on the 21st of May 2024. Notice that parts of the globe, especially near the equator have not been observed. This image was produced using NASA Worldview (https://go.nasa.gov/46SaYyJ).

Forecasting the weather or evolution of any other system is formulated as an initial value problem where past observations are used to predict an unknown future state of the system. A different formulation can be how heat spreads over time in different types of frying pans from known information of the pan's materials, their

heat conduction properties, and that the stove gives off constant heat. In general the scenario is predicting the effect (future atmospheric temperature distribution, etc.) of some given causes (current and past weather, etc.). This scenario is termed the forward problem. The inverse problem on the other hand solves for an unknown parameter using other known parameters and observations of the partial solution such as temperature field at the object's surface. Traditional methods used to solve these problems utilized knowledge of the exact equations to numerically solve PDEs. As an example, the Finite Difference Method (FDM) approximates the solution by substituting the partial derivatives with finite differences and manipulating the equation such that the solution can be computed. The inverse problem on the other hand is determination of initial conditions or other parameters from observed state of the system. For example determining the heat source distribution given the temperature distribution at some point in time. One traditional approach to this would have meant solving the forward problem from an initial guess of the parameter and then evaluating some cost function such as how close the predicted solution is to the observed one. As expected, this would require many evaluations of the forward solver. This means that the cost of the solver would be greatly multiplied, emphasizing the importance of an efficient solver.

Traditional numerical solvers have enjoyed many decades of development due to their long history. There are many general approaches to solve PDEs and many more very specific approaches. Other than FDM, some widely used approaches include Finite Element Methods (FEM), Finite Volume Methods (FVM), Collocation Methods, and Spectral Methods. FEM and FDM are both mesh based approaches, meaning they rely on discretization of the computational domain. There are several challenges associated with this. First, irregular domains such as bio-inspired materials like bone, spider silk, or aggregate materials like gravel pose a challenge due to the complexity of the domain geometry (Buoni & Petzold, 2007; Gaul et al., 1991; Jia et al., 2024). Also, irregular domains which create large deformations or mesh entanglement cause these methods to become ineffective (J.-S. Chen et al., 2017). While there are strategies to mitigate this, by definition they are an additional layer of difficulty to the process. Second, multiscale applications where the micro and macro scales are both important require fine meshes such that the small scale structures are adequately simulated. This creates meshes with very large number of points that are very resource intensive (Buoni & Petzold, 2007). Third, a single evaluation of traditional mesh-based solvers may not be very costly, however multiple evaluations can add up. This is very apparent

in inverse problems where the solver is queried multiple times to solve the forward problem in order to obtain parameter functions. Therefore, in problems where these issues important or resources are limited, mesh-free methods may be preferred. As an example, the spectral method solves PDEs by formulating the solution as a linear combination of global basis functions like the Fourier series. This can be likened to how music combines different sound waves to produce the overall sound. For some function s, the approximation s^* gets closer to the original with more linear combinations of basis functions. The complex formulation of the Fourier series is presented in equation (1.2). With this approach, the approximated function is characterized completely by its coefficients c_k. This fact is exploited by the spectral method to solve differential equations. The solution function can be approximated by finding the mapping between input function coefficients and solution function coefficients. The mapping between a function s and its derivative s' can be found using the derivative equation from their coefficients leading to $\hat{s}_k = \hat{s}'_k/(2\pi ik)$. Practically this would be done with a finite number of coefficients ($k < \infty$) and the coefficients $\hat{s}'_k$ are obtained using a Discrete Fourier Transform (DFT) algorithm like the Fast Fourier Transform (FFT).

$$s \approx s^* = \sum_k \hat{s}_k e^{2\pi ikx} \tag{1.2}$$

This leads us to the fourth challenge with traditional methods which is that they require prior knowledge of analytic forms of PDEs. This is because traditional solvers use the equations to formulate solutions. This makes traditional numerical approaches unsuited to problems where the governing equations are unknown or partially known. These challenges altogether are some of what weather forecasting faces; NWP has the immense task of modeling multiple scales of the Earth's atmosphere while accounting for features of physical systems that are still not fully understood. Many other fields such as epidemiology (Brauer et al., 2019) and ecology (Holmes et al., 1994; Turchin, 2001) also face these challenges. As with many other fields, at some point in time the governing equations of many systems were not known. This has motivated research into alternative methods that do not completely rely on prior knowledge, are mesh free, and fast enough when solving forward problems.

Machine Learning for PDEs

With the increasing prevalence of machine learning methods and their use in more and more fields, research into their use for scientific computing has taken off in recent years. While statistical modeling has already been widely used in areas such as physical constants, stellar population studies, risk assessments of events such as earthquakes and coronal mass ejections (Anselmo & Pardini, 2005; Berliner, 2003; Bernardi et al., 2022; Reinhardt et al., 2016; Spanos, 2006; Uzan, 2003), the dominant approach for forward modeling or inverse modeling has remained physics based numerical models. Machine learning has provided an alternative approach to model the solutions of PDEs. In their work, Aarts and Van Der Veer (2001) utilized neural networks to approximate each term of PDEs describing damped and undamped free vibrations and substituting them into the PDEs and associated initial conditions. The network parameters were then optimized to reduce the PDE residual and boundary condition loss using evolutionary algorithms. This approach was taken in order to make machine learning models more transparent which at the time was being pursued because of the high cost of optimizing uncertainties in water management numerical simulators. However, since this method approximates the mapping between coordinates and the values of a function and their derivatives, retraining would be necessary for changes to the function itself. This could become very costly as retraining costs accumulate. A more recent approach that also utilizes soft constrains from PDE residuals is termed physics informed neural network (PINN) (Raissi et al., 2019). The authors propose a framework that leverages advancements in computing, namely automatic differentiation (AD) techniques made readily available by modern machine learning libraries. In general, PINNs use AD to compute each term of the PDE from the output of the model and this is then substituted into the PDE to in order to compute the residuals and loss from boundary conditions. The network residual and boundary loss are then weighted and summed with the data loss. For a neural network $\hat{u}(\mathbf{x},t)$ approximating the real solution $u(\mathbf{x},t)$, the residual loss for the heat equation in equation (1.1) is equation (1.3). There are several advantages of incorporating physics knowledge into the model including regularization of the model outputs to be more consistent with physics, faster convergence, and less to no data required depending on whether the network is trained in a manner that is supervised, self-supervised, or a combination of both. One issue with using AD to compute the residual is that the network input needs to be the independent variable (i.e. coordinates, time, etc.). This once again means that if one wants to compute a different

solution, the network needs to be retrained.

$$\mathscr{L}_{PDE} = \left(\frac{\partial \hat{u}(\mathbf{x},t)}{\partial t} - \nabla \cdot (\alpha \nabla \hat{u}(\mathbf{x},t)) \right)^2 \tag{1.3}$$

Learning PDEs with CNNs

Other works utilize convolutional neural networks (CNN) to compute the solution from input functions such as forcing terms or initial conditions. This approach generally means discretizing the functions on a grid and using these as training data. One study by R. Wang et al. (2020) predicts turbulent flow using spatial and temporal decomposition and a specialized U-Net, an architecture based on CNNs, to predict the velocity field from the decomposition of the previous velocity field. Part of the loss function is a regularization term for zero divergence in the velocity field to enforce incompressible fluid flow. This term was calculated using finite differences since auto differentiation is not applicable in this situation. Finite differences was also utilized in another CNN based fluid flow upscaling model by Gao et al. (2021b) to compute the residual terms of the steady incompressible Navier-Stokes equation. This model also inferred unknown physical parameters such as boundary conditions. However, this approach would mean the model would need to scale as a quadratic in 2D, cubic in 3D, and much steeper in higher dimensions. Outside fluid dynamics, the combination of specialized CNNs and finite differences or another numerical differentiation method have been used for many other PDEs including Poisson's equation for temperature fields (Gao et al., 2021a; Zhao et al., 2023), velocity models from seismic data (Muller et al., 2023), and seismic response of structures (Ni et al., 2022; Zhang et al., 2020). While the use of CNNs mean that discretization is implied, solutions of different initial conditions or parameter functions can be computed by inference and no retraining is required. This property is especially useful for many-query problems such as computing gradients for inverse problems.

Operator Learning

The mapping between discretized functions done by CNNs are related to an alternative approach that starts by viewing PDEs as operators, which are generalized mappings between spaces. One group of familiar operators are functions which maps between spaces of scalar values or vector values. PDEs on the other hand are operators

that map between function spaces. A simple example is the derivative. The derivative takes in a function and returns the derivative of said function. In other words it is an operator that maps between the space of all functions to the space of derivatives of those functions. Another way to view operators starts by viewing functions as infinite dimensional vectors. Where elements in the vector are the function's value evaluated at every point in space. The operator can be seen as a vector function mapping between these infinite dimensional vector spaces. Operators are important because a field of research has sprung up around this mathematical concept. Operator learning is the use of machine learning to learn operators using data driven approaches. As an analogy, function regression traditionally has been used to approximate the mapping between input values such as coordinates and output values of functions evaluated at said coordinates. In the case of operator learning, the mapping between function spaces are approximated. The aforementioned approaches using CNNs does this directly using the values of functions at discrete points. There are other approaches like DeepONet that does not require the uniform grid like CNNs (Lu et al., 2021). This architecture instead uses both input functions and coordinates as inputs. The output is the output function evaluated at the coordinates provided. This architecture is based on an extension for deep learning of the universal operator approximation theory for neural networks first proposed almost three decades ago at the time of writing by T. Chen and Chen (1995). The proposed architecture is composed of two subnetworks, where one termed the trunk $\hat{\mathbf{T}}(\mathbf{x},t)$learns the latent mapping for coordinates and the other network termed the branch $\hat{\mathbf{B}}(\mathbf{f})$ learns the latent mapping for the input function f. The two latent mappings are combined through a dot product to obtain the approximated output function value $u(\mathbf{x},t)$. This is formulated in equation (1.4).

$$u(\mathbf{x},t) \approx \hat{G}(\mathbf{f})(\mathbf{x},t) = \hat{\mathbf{B}}(\mathbf{f}) \cdot \hat{\mathbf{T}}(\mathbf{x},t) \tag{1.4}$$

Fourier Neural Operators (FNO) is an alternative avenue for learning operators by utilizing the fact that functions can be decomposed into linear combinations of basis functions, namely trigonometric basis in this particular case (Li et al., 2021). With this method the input function value is mapped to its corresponding output function value. This is done by first lifting the input function value to a higher dimension using a neural network and this is then passed through blocks composed of a Fourier transform, then a linear transform and filtering of higher modes, and finally the inverse Fourier transform. These blocks are stacked to a desired depth and finally another network

projects the outputs to the target dimension. The reason a linear can be used is that differentiation is multiplication in the Fourier domain. One drawback with FNO is the requirement that output functions are not parameterized by coordinates and therefore is implicitly relative to the input function coordinates. To avoid this issue, Fanaskov and Oseledets (2023) reframes the problem by directly utilizing the coefficients of Fourier or Chebyshev basis. The model, termed Spectral Neural Operator (SNO) is trained on features of input function coefficients which are computed using Fourier or Chebyshev transforms and labels of output function coefficients using the same transforms. The authors point out one motivation for this approach which is that training neural networks on discretized data may not be ideal because unexpected outputs such as non-smooth interpolation may happen when the network is trained on one grid size and evaluated other grid sizes. With SNO, the interpolation of the function is smooth due to interpolation being done by Fourier basis functions which are sines and cosines for example. In a similar study, Du et al. (2024) extends the concept of mapping coefficients by proposing residuals in the spectral domain and leveraging Parseval's Identity to compute the spectral analog to the loss term in PINNs. This allows for self supervised learning in the spectral domain. The same benefits incorporating physics into PINNs also apply here without the pain points introduced by discretized model inputs and outputs. As a whole, operator learning creates an alternative approach that addresses the issue of retraining or recomputing the solution model. In addition, due to its data based approach, even systems with partially or fully unknown governing equations may be simulated.

A persistent challenge with all these approaches is the issue of optimization. While neural networks are modular and expressive which is proven by the universal approximation theorem (Cybenko, 1989; Hornik et al., 1989), their loss function present many local minima meaning it is non-convex. This can be mitigated by using advanced optimization techniques that can find a local minima close enough to the global minima such as Adam (Shrestha & Mahmood, 2019; Soydaner, 2020). However, the addition of PDE residuals into the loss function have worsened the highly non-convex loss landscape issue (Basir & Senocak, 2022; Krishnapriyan et al., 2021; Rathore et al., 2024). These problems range from the disparity in size of boundary and residual loss gradients to the fact that incorporation of residuals and boundary conditions themselves create a much more complex loss landscape. As a result, it is desirable to utilize a different machine learning algorithm that possesses a convex

loss landscape. One family of such algorithms are Support Vector Machines (SVM) (Vapnik, 2000). The appeal of SVMs are the fact that the model is formulated as a quadratic programming problem. This means there are strong guarantees for convergence, generalization, and complexity. Another formulation called Least Squares Support Vector Machines (LSSVM) reformulates the problem as a linear system (Suykens, 2005). This leads to an easier problem that can be computed faster by well established algorithms like the many implementations of least squares solvers. Another advantage of the linear formulation is that this can be easily parallelized to exploit hardware like graphics processing units more widely known as GPUs in contrast to the commonly used Sequential Minimal Optimization (SMO) used for SVMs with quadratic objective functions.

The advantageous properties of SVM based methods have attracted research into their use for solving PDEs. An early work using SVMs to solve PDEs by Youxi Wu et al. (2005) introduced a method for solving the forward problem of Electro-Impedance Tomography. This work solved for the mathematical model of EIT which is given by Maxwell's equations by modeling the trial function as using an ε-SVR model. Another approach much more similar to PINNs was presented by Mehrkanoon and Suykens (2015). The residual and initial/boundary conditions are imposed as equality constraints on an LS-SVM objective function. A different study by Leake et al. (2019), the incorporation of physics into the model is done slightly differently by utilizing the theory of functional connections to directly embed constraints into the solution. This means that the proposed method would satisfy the boundary condition exactly. However, the authors point out that for PDEs in higher dimensions deriving and implementing this method can become cumbersome. These approaches, however, do not learn the PDE operator itself. Meaning they are also not practical for many-query problems.

Operator Learning for Weather Forecasting

In terms of weather forecasting, operator learning has been applied in terms of initial value problems. This problem formulation is reminiscent of time series prediction problems widely found in machine learning research. Researchers Kurth et al. (2023) developed FourCastNet which utilized Adaptive Fourier Neural Operator (AFNO), a transformer based model containing the previously mentioned FNO

computational blocks by Li et al. (2021). This model was then able to be trained in a massively parallel manner. In a comparison with a traditional model called the Integrated Forecasting System from the European Center for Medium Range Weather Forecasts (ECMWF), FourCastNet is faster and much more efficient in terms of inference time, resulting in about 80,000 times speed up for a 100-member ensemble forecast. This is while performing much better than a previous deep learning approach. In another study, Bonev et al. (2023) proposed a variation on neural operators called Spherical Fourier Neural Operator (SFNO) which exploited the spherical nature of global forecasting by using Spherical Harmonic Transform (SHT) in place of Fourier Transform. This model when compared to AFNO and FNO, produced no visible artifacts in autoregressive rollouts for long range forecasting. In terms of forecasting, the model shows outcomes that matches the IFS which is a big leap forward in parity for traditional and machine learning based methods.

1.2 Problem Statement

The problems this work sets out to solve based on section 1.1 are:

1. What is the formulation a computational model for operator regression and therefore solving PDEs in the spectral domain using support vector machines?
2. Can the model learn the relationships represented by PDEs? And how does it perform on different problems?
3. How can one interpret the learned model?

1.3 Aims

Based on the stated problems in section 1.2, this study aims to acomplish the following:

1. The design and implementation of a computational model that maps coefficients in the spectral domain using Least Squares Support Vector Regression (LSSVR).
2. Proof of the model's learning ability using three different problems.
3. Interpretation the model results and why some predictions turn out the way they do.

1.4 Contribution

In achieving the aims of this study the following contributions are made:

1. A novel use LSSVR which has a convex objective to learn solution operators of partial differential equations and operators in general.
2. Interpretation of machine learning model trained on operator data.

1.5 Limitations

This work is limited to the following:

1. Functions the model works with are only continuous functions.
2. The basis functions are limited to Fourier basis.
3. Modeled fields are compact or dense meaning not sparse. Sparse observations or other data are assimilated using other methods.

1.6 Sistematika Penulisan

CHAPTER II

KAJIAN PUSTAKA

Bab ini mengulas secara rinci konsep-konsep dasar yang berkaitan dengn pekerjaan penelitian TA dan deskripsi studi pustaka yang dilakukan. Judul bab tidak harus seperti yang dituliskan, melainkan dapat lebih fleksibel yang mencerminkan isi paparan pada bab ini. Demikian halnya dengan judul sub bab.

2.1 Fourier Transform and Series

Complex numbers are numbers consisting of real and imaginary components. Complex numbers are written as in equation (2.1) with a and b being the real and imaginary components respectively. The imaginary component is multiplied by the imaginary unit $i = \sqrt{-1}$.

$$c = a + bi \tag{2.1}$$

$$\tag{2.2}$$

("Discrete Fourier Transform," n.d.)

$$c_k = \sum_{n=0}^{N-1} f_n e^{-i2\pi kn/N} \tag{2.3}$$

$$f_n = \sum_{k=0}^{N-1} c_k e^{i2\pi kn/N} \tag{2.4}$$

2.2 Least Squares Support Vector Machine

An arguably fundamental model widely used whether in pedagogical settings or otherwise is the support vector machine. It dates back to works by Vapnik & Lerner in 1963 (Recognition of Patterns with help of Generalized Portraits) and V. N. Vapnik & A. Ya. Chervonenkis in 1964 (A note on one class of perceptrons/On a perceptron class). As the development on SVM continued, what originally was a model for

classification of separable data generalized to regression tasks as well Vapnik (2000 The Nature of Statistical Learning Theory).

2.2.1 Disadvantages

However, the main disadvantage of LSSVMs are the fact that they do not have the sparse property of SVMs which can leave performance on the table. A simple mitigation can be done by filtering training samples with small absolute values of lagrangian multipliers (Haifeng Wang & Dejin Hu, 2005).

To derive the least squares support vector regression (J.A. Suykens LSSVM Book) model we start with the linear expression:

$$y = W^{\mathsf{T}}\mathbf{x} + b \tag{2.5}$$

$$\min_{W,e} J(W,e) = \frac{1}{2}W^{\mathsf{T}}W + C\frac{1}{2}\sum_{k=1}^{n} e_k \tag{2.6}$$

Such that

$$y_k = W^{\mathsf{T}}\mathbf{x}_k + b + e_k \qquad k = 1,\ldots,n \tag{2.7}$$

$$L(W,b,e;\alpha) = \frac{1}{2}W^{\mathsf{T}}W + C\frac{1}{2}\sum_{k=1}^{n} e_k + \sum_{k=1}^{n}\alpha_k\left(W^{\mathsf{T}}\mathbf{x}_k + b + e_k - y_k\right) \tag{2.8}$$

Derive the KKT system

$$\begin{aligned}
\frac{\partial L}{\partial W} &= 0 \rightarrow W = \sum_{k=1}^{n} \alpha_k x_k \\
\frac{\partial L}{\partial b} &= 0 \rightarrow \sum_{k=1}^{n} \alpha_k = 0 \\
\frac{\partial L}{\partial e_k} &= 0 \rightarrow \alpha_k = C e_k \qquad\qquad k = 1, \ldots, n \\
\frac{\partial L}{\partial \alpha_k} &= 0 \rightarrow W^{\intercal} \mathbf{x}_k + b + e_k - y_k = 0 \qquad k = 1, \ldots, n
\end{aligned} \tag{2.9}$$

After eliminating W and e, with $\mathbf{1}_n = \langle 1, \ldots, 1 \rangle$, $\mathbf{y} = [y_1, \ldots, y_n]$, and $\alpha = [\alpha_1, \ldots, \alpha_n]$ the solution is as follows in block matrix notation

$$\begin{bmatrix} 0 & \mathbf{1}_n^{\intercal} \\ \mathbf{1}_n & \Omega + \frac{I}{C} \end{bmatrix} \begin{bmatrix} b \\ \alpha \end{bmatrix} = \begin{bmatrix} 0 \\ \mathbf{y} \end{bmatrix} \tag{2.10}$$

The solution in eq. (2.10)

Algorithm 1 LSSVR Training

procedure SOLVELSSVR($\mathbf{X}, \mathbf{y}, \gamma$)
  $\Omega \leftarrow [[]]$ ▷ Construct matrix of inner products in high dimensional space
  for $k = 0 \rightarrow n$ **do**
    for $l = 0 \rightarrow n$ **do**
      $\Omega_{k,l} \leftarrow K(\mathbf{X}_k, \mathbf{X}_l)$
    end for
  end for
  $\mathbf{H} \leftarrow \Omega + \frac{\mathbf{I}}{\gamma}$
  $\mathbf{A} \leftarrow [[]]$ ▷ Construct left-hand side matrix
  $\mathbf{A}_{0,0} \leftarrow 0$
  for $k = 0 \rightarrow n$ **do**
    $\mathbf{A}_{k+1,0} \leftarrow 1$
    $\mathbf{A}_{0,k+1} \leftarrow 1$
  end for
  for $k = 0 \rightarrow n$ **do**
    for $l = 0 \rightarrow n$ **do**
      $\mathbf{A}_{k+1,l+1} \leftarrow \mathbf{H}_{k,l}$
    end for
  end for
  $\mathbf{B} \leftarrow []$ ▷ Construct left-hand side of the equation
  $\mathbf{B}_0 \leftarrow 0$
  for $k = 0 \rightarrow n$ **do**
    $\mathbf{B}_{k+1} \leftarrow \mathbf{y}_k$
  end for
  $\mathbf{A}^\dagger \leftarrow pseudoInverse(\mathbf{A})$ ▷ Compute solution using pseudo inverse
  $\mathbf{S} \leftarrow \mathbf{A}^\dagger \mathbf{B}$
  $b \leftarrow \mathbf{S}_0$
  for $k = 0 \rightarrow n$ **do**
    $\alpha_k \leftarrow \mathbf{S}_{k+1}$
  end for
  return α, b
end procedure

The basic pseudocode from the LSSVM Equation for function regression is defined in algorithm 1 for a training set of length n, features $\mathbf{X}$, and labels $\mathbf{y}$. Training the LSSVM means computing the values of langrange multipliers α and bias b. K is the kernel function used to compute the inner products in high dimensional space, here we assume the RBF kernel. $\mathbf{A}$ is a matrix of size $n+1$ by $n+1$. $\mathbf{H}$ is a matrix of size n by n. $\mathbf{I}$ is the identity. $\mathbf{B}$ is a vector of size $n+1$. $\mathbf{S}$ is a vector of size $n+1$.

After training the model can be used for prediction of unseen features. The pseudocode for prediction is shown in algorithm 2 for prediction features $\mathbf{U}$ with p samples. The trained model uses the training features themselves $\mathbf{X}$ with n samples, the learned multipliers of training points α, and the bias b.

Algorithm 2 LSSVR Prediction

Input: $\mathbf{U}, \alpha, \mathbf{X}, b$
Output: $\mathbf{v}$

$\Omega \leftarrow [[]]$ ▷ Construct matrix of inner products in high dimensional space
for $k = 0 \rightarrow p$ **do**
    for $l = 0 \rightarrow n$ **do**
        $\Omega_{k,l} \leftarrow K(\mathbf{U}_k, \mathbf{X}_l)$
    end for
end for
$\mathbf{v} \leftarrow \Omega\alpha + \mathbf{1}_m b$

In this exmple we will be using the function $2x^2 + 4$. The values of this function can be seen in Table 2.1.

No	x	y
1	0.0	4.0
2	0.33...	4.22...
3	0.66...	4.88...
4	1.0	6.0

Table 2.1: Example data of function $2x^2 + 4$

For $\Omega_{i,j} = K(x_i, x_j) = exp\left(-\frac{\|x_i - x_j\|^2}{2\sigma^2}\right)$

For example, with $\sigma = 1$, $x_i = 0.0$, & $x_j = 0.33\ldots$

$$\begin{aligned} K(0.0, 0.33) &= exp\left(-\frac{\|0.0 - 0.33\|^2}{2(1)^2}\right) \\ &= exp\left(-\frac{0.33^2}{2}\right) \\ &= 0.9460 \end{aligned} \tag{2.11}$$

$$\Omega \leftarrow \begin{bmatrix} 1.0000 & 0.9460 & 0.8007 & 0.6065 \\ 0.9460 & 1.0000 & 0.9460 & 0.8007 \\ 0.8007 & 0.9460 & 1.0000 & 0.9460 \\ 0.6065 & 0.8007 & 0.9460 & 1.0000 \end{bmatrix} \tag{2.12}$$

$$\mathbf{I}\frac{1}{\gamma} \rightarrow \mathbf{I}\frac{1}{5} \rightarrow \begin{bmatrix} 0.2000 & 0.0000 & 0.0000 & 0.0000 \\ 0.0000 & 0.2000 & 0.0000 & 0.0000 \\ 0.0000 & 0.0000 & 0.2000 & 0.0000 \\ 0.0000 & 0.0000 & 0.0000 & 0.2000 \end{bmatrix} \tag{2.13}$$

$$\Omega + \mathbf{I}\frac{1}{5} \rightarrow H \rightarrow \begin{bmatrix} 1.2000 & 0.9460 & 0.8007 & 0.6065 \\ 0.9460 & 1.2000 & 0.9460 & 0.8007 \\ 0.8007 & 0.9460 & 1.2000 & 0.9460 \\ 0.6065 & 0.8007 & 0.9460 & 1.2000 \end{bmatrix} \tag{2.14}$$

$$A \rightarrow \begin{bmatrix} 0.0000 & 1.0000 & 1.0000 & 1.0000 & 1.0000 \\ 1.0000 & 1.2000 & 0.9460 & 0.8007 & 0.6065 \\ 1.0000 & 0.9460 & 1.2000 & 0.9460 & 0.8007 \\ 1.0000 & 0.8007 & 0.9460 & 1.2000 & 0.9460 \\ 1.0000 & 0.6065 & 0.8007 & 0.9460 & 1.2000 \end{bmatrix} \tag{2.15}$$

$$B \rightarrow \begin{bmatrix} 0.0000 \\ 4.0000 \\ 4.2222 \\ 4.8889 \\ 6.0000 \end{bmatrix} \tag{2.16}$$

$$A^{\dagger} \rightarrow \begin{bmatrix} -0.8994 & 0.4348 & 0.0652 & 0.0652 & 0.4348 \\ 0.4348 & 2.0686 & -1.6490 & -0.5292 & 0.1096 \\ 0.0652 & -1.6490 & 3.3774 & -1.1992 & -0.5292 \\ 0.0652 & -0.5292 & -1.1992 & 3.3774 & -1.6490 \\ 0.4348 & 0.1096 & -0.5292 & -1.6490 & 2.0686 \end{bmatrix} \tag{2.17}$$

$$A^{\dagger}B \rightarrow S \rightarrow \begin{bmatrix} 4.9421 \\ -0.6177 \\ -1.3737 \\ -0.5625 \\ 2.5538 \end{bmatrix} \tag{2.18}$$

$$b \rightarrow 4.9421 \tag{2.19}$$

$$\alpha \rightarrow \begin{bmatrix} -0.6177 \\ -1.3737 \\ -0.5625 \\ 2.5538 \end{bmatrix} \tag{2.20}$$

Prediction

$$U \rightarrow \begin{bmatrix} 0.3 \\ 0.2 \\ 0.5 \end{bmatrix} \tag{2.21}$$

$$\Omega \rightarrow \begin{bmatrix} 0.9560 & 0.9994 & 0.9350 & 0.7827 \\ 0.9802 & 0.9912 & 0.8968 & 0.7261 \\ 0.8825 & 0.9862 & 0.9862 & 0.8825 \end{bmatrix} \tag{2.22}$$

$$\Omega\alpha \rightarrow \begin{bmatrix} -0.4904 \\ -0.6170 \\ -0.2008 \end{bmatrix} \tag{2.23}$$

$$\Omega\alpha + b\mathbf{1}_m \rightarrow v \rightarrow \begin{bmatrix} 4.4516 \\ 4.3251 \\ 4.7413 \end{bmatrix} \tag{2.24}$$

Where $\mathbf{1}_m$ is a vector of 1s with the length of U.

CHAPTER III

RESEARCH METHODOLOGY

3.1 Research Design

This study is carried out under the framework of a research design. In this section, this design will be laid out and explained. The design includes the process from the beginning to the end of the overall study. The research design is visually depicted in figure 3.1.

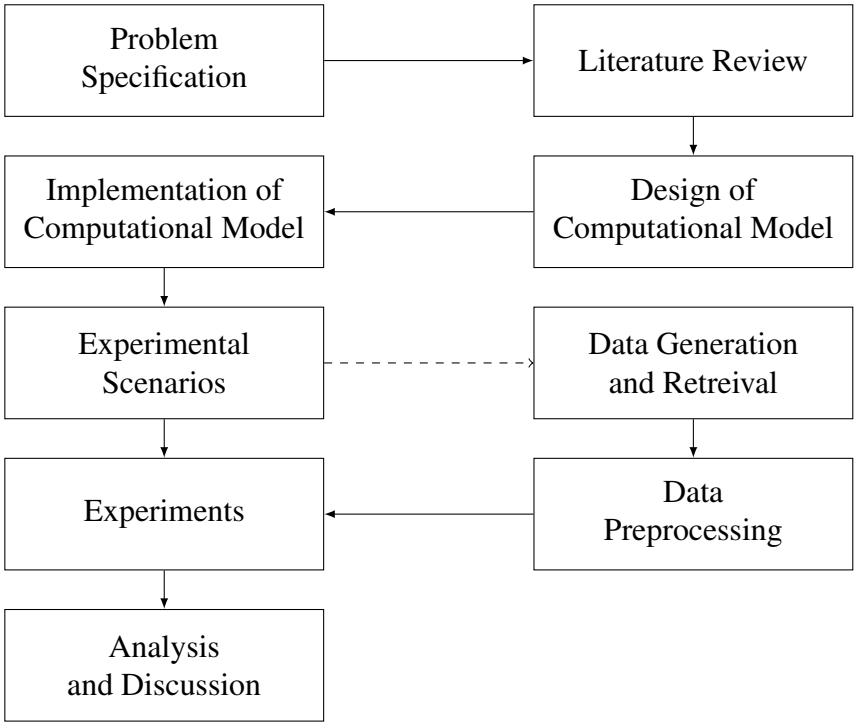

Figure 3.1: Research design diagram

The study is carried out in 9 main phases. Each phase has a specific aim to accomplish such that the subsequent phases are able to proceed. Each phase is explained as follows:

1. Problem Specification

   In this phase, relevant literature of related works and other supporting materials

will be reviewed to lay the groundwork of this study. Specifically, the literature review will encompass partial differential equations and their real world associations, traditional methods employed to solve them, systems with partially known or unknown governing equations, machine learning approaches to the problem, least squares support vector machines, performance metrics, and tools that will be used such as the PyTorch library.

2. Design of Computational Model

   This phase of the study is allocated to the design of the computational model based on the literature that has been reviewed. The design of the overall process includes data retrieval, preprocessing, and the core spectral regression model itself.

3. Implementation of Computational Model

   After the computational model design is completed, the model is implemented in the Python Language using the Pytorch library as a core component. Implementation of the computational model is done using an iterative software development model. This development model was chosen due to its adaptability to unexpected challenges which is necessary because of the challenges and unknowns with developing a novel method.

4. Planning of Experimental Scenarios

   To properly gauge the performance of the proposed method at approximating operators, specifically the solution operator of partial differential equations, experimental scenarios are developed in this phase. Specifically, the scenarios serves three goals which are proof of concept or validation that the method is able to learn operators, a case study of a more complex system with real world data, and a using the model as a surrogate. Together, these experimental scenarios determine the applicability of the model to the problem. In addition, the model will be compared to a baseline model in order to put into context the proposed model's performance. In addition, kernel-input correlation matrices and input-Lagrangian multiplier inner product matrix will also be computed.

5. Data Generation and Retrieval

This phase of the study is tied to the experimental scenarios that have been developed. After determination of the scenario specifics, the data that will be used for training, validation, and testing of the model in each scenario will be either generated or retrieved from an external source. In addition, in each scenario the hyperparameters of the model will be determined using Bayesian optimization as an alternative to the traditional grid search method.

6. Data Preprocessing

   The next phase after data generation or retrieval is preprocessing. This is a crucial step in allowing the core LSSVR to learn the mappings in spectral space. In order to do this, the data will need to be reshaped, and important features selected for. Finally, inputs to the LSSVR will need to be normalized or scaled such that the LSSVR model can much more easily learn the data.

7. Experiments

   This phase of the study executes the experimental scenarios that was determined previously. The preprocessed data will be used in accordance to the preplanned scenarios.

8. Analysis and Discussion

   The final phase of the study is the analysis and discussion of the results. Analysis of each experimental scenario will assess the extent of the model's capabilities. Another component of the analysis is interpretation the trained model and how it comes to the predictions that it makes. The discussion will also touch on the hyperparameter optimization and comparisons with the baseline model. This will show how the model performs differently compared to the baseline.

3.2 Literature Study Method

As a basis for this study, information surrounding the topic is collected from literature sources such as books, journal articles, and other academic works like dissertations. The tools that are used to find these sources include Google Scholar and Google Search. The search terms used start with two terms which are partial differential equations and machine learning. Based on reading the most relevant literature, further search terms

are created from variants of previous search terms combined with terms from literature that has been found.

3.3 Data Generation and Retrieval Method

Data to be used in this study are acquired in two different ways. The first method is data generation. This is motivated by the fact that some partial differential equations do not have much open and accessible real world data available. As such the systems are simulated using the equations themselves. In simple scenarios like computing the antiderivative u of some function f, this can be done by randomly generating u and then taking their derivatives to compute f. The random function generation itself is done by generating random coefficients for basis functions like the Fourier series. Once all functions are generated, random noise is added to ensure that the model is also robust towards inexact measurements. A diagram illustrating the process is shown in figure 3.2.

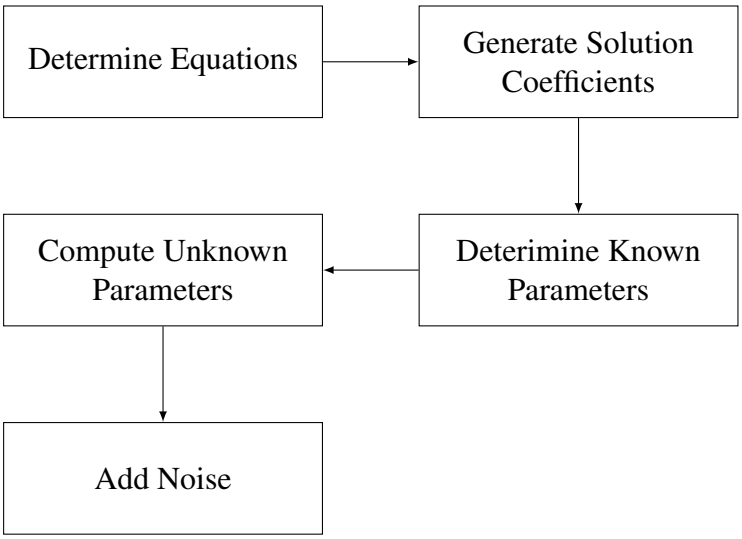

Figure 3.2: Data generation diagram

Data retrieval is the other option which in this case is used to retrieve data for weather prediction. Based on the scenario the data is to be used for, relevant subsets of the dataset is retrieved to a working machine. This study specifically uses a dataset provided by the European Center for Medium Range Weather Forecast (ECMWF) named ERA5 hourly data on single levels from 1940 to present (C3S, 2018). The

first step is selecting a geographical area to study, time period, NetCDF4 data format, and variables such as temperature at 2 meters above the surface. Then the second step is specifications are then used to request the data through the climate data store application programming interface. The downloaded data is then parsed using the Xarray library and preprocessed.

3.4 Computational Model Implementation Method

Implementation of the computational model follows an iterative development model. This model basically consists of repeated cycles or iterations of software development. Each cycle is loosely based on the waterfall development model, namely the processes of requirement gathering, analysis & design, implementation, and testing. This iterative property is crucial for this study because all the requirements cannot be known beforehand. This model minimizes the risk in developing complex software with partially known initial requirements. A diagram of the model can be seen in figure 3.3.

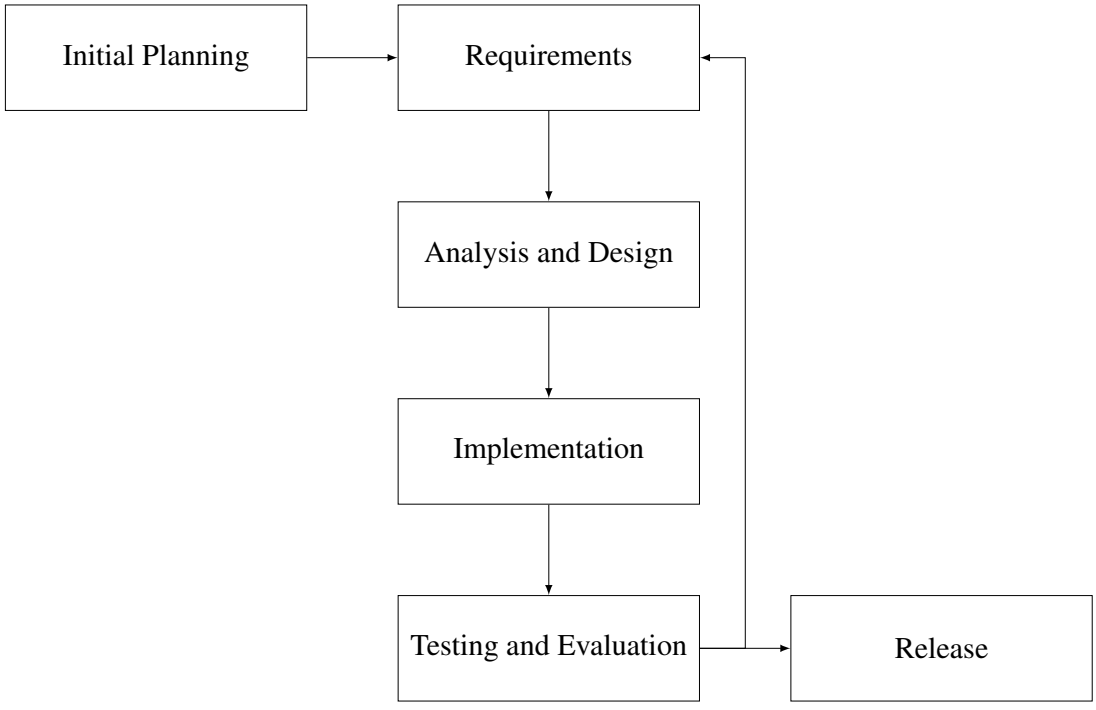

Figure 3.3: Iterative development model

This development model was adapted from Bittner and Spence (2006). Each process in the model is explained as follows:

1. Initial Planning

   The first process of the iterative development model sets up the parameters for the iterative development. These parameters are the broad scope of the project and initial requirements such as core components like LSSVR. The initial requirements are crucial in guiding the rest of the development as more requirements are gathered. The initial planning also determines technical choices like tooling and choice of language. The planning process also includes a rough architecture based in initial requirements.

2. Requirements

   This process separates out the backlog of requirements into those that will be worked on in the current iteration. These requirements ideally share some functionality in order to allow the same context to be retained within the iteration which reduces the burden of context switching.

3. Analysis and Design

   This process an analysis of the requirements of the current iteration is performed. This involves determining the constraints and goals for each requirement. Constraints also need to consider previous iterations such that the requirements can be fulfilled effectively and efficiently without regressing progress that has been made such as breaking existing functionality. From this analysis, the design is updated so that the requirement can be fulfilled. The design itself informs how the code should be structured. The interfaces used in the code are also specified.

4. Implementation

   The implementation process applies the design that has been produced. In addition to implementing the program, this process also implements tests which validate and verify the produced code. In the case of complex pieces of the design, an approach of creating tests and assertions first is taken. This way, the code can be run quickly and fail immediately to allow a quicker convergence on the intended functionality.

5. Testing and Evaluation

   Once the design is implemented, tests that have been created are run. Each

feature is tested in an integrated manner to expedite the process while still providing enough confidence in the software. The results of the testing process are evaluated and any failed tests are resolved whether by reimplementation or reassessment of the correctness of the tests. Any missing functionality or feature discovered during evaluation are added to the backlog of requirements.

6. Release

   After an iteration, the current version of the software is released. The iterative nature of this development model necessitates the use of a versioning system. As such each release can be identified by a version number loosely based on semantic versioning (Preston-Werner, n.d.). This version numbering system consists of major number that indicates breaking changes, minor numbers which indicate features and non-breaking changes, and lastly patch numbers are used for fixes. A version number is read as `MAJOR.MINOR.PATCH`. During active development, only major version 0 will be used to prevent too many major versions. The released software is hosted in its own GitHub repository at https://github.com/nidduzzi/SpectralSVR.

3.5 Research Tools

The tools that are used in this study can be categorized into hardware and software. The following are hardware that are used in this study:

- Kaggle CPU Kernel ("Getting Started on Kaggle | Kaggle," n.d.)
  - 4 Cores Intel Xeon
  - 30 Gigabytes RAM
  - 20 Gigabytes Working storage
- Kaggle GPU Kernel ("Getting Started on Kaggle | Kaggle," n.d.)
  - 4 Cores Intel Xeon
  - 29 Gigabytes RAM
  - 1 Nvidia P100 GPU

  - 20 Gigabytes Working storage
- Personal Computer
  - Intel i5-8300H
  - 16 Gigabytes RAM
  - Nvidia GeForce GTX 1060 Mobile
  - 1.5 Terabytes Storage

The software tools used in this study are the following:

- Python
- Jupyter Notebook
- Git
- Poetry Python package manager
- Web Browser
- LaTeX

CHAPTER IV

RESULTS AND DISCUSSION

This chapter will elaborate on the results of the study and relevant phases for analysis. This chapter is organized into five sections which are the results of data generation, data retrieval, design of computational model, implementation of computational model, experimental scenarios, and the experiments themselves.

4.1 Data Generation

This study uses two data acquisition approaches. The first approach which is discussed in this section is data generation. This process involves manufacturing data randomly in such a way that they obey the PDEs to be modeled. The generated data consists of features and labels. These features and labels in the context of PDEs are parameters and the solution of the PDEs, respectively. The PDEs enforce a relationship between parameters and the solution. This relationship is implicitly encoded into the features and labels, which is what machine learning models can learn. Because the solution and parameters to PDEs are functions and there are many kinds with different properties, generating all the different kinds of functions is a difficult task. This is why this study focuses on Fourier functions. This means that out of the space of all functions F which include categories such as polynomials $f(x) = a_n x^n + \cdots + a_1 x + a_0$ where $f \in F$, and a_n are constants; we only consider the subset of functions $U \subset F$ which are of the form $u(x) = \sum_k^m c_k e^{2\pi i k \frac{x}{P}}$.

Using the subset of Fourier functions has several benefits which has motivated the choice. First these functions are characterized purely by their coefficients c_k, meaning there is no need to store discretized values which potentially saves space and computation. The second benefit is that other functions such as polynomials can be approximated by them using the Fourier transform. This means that despite limiting the set of functions to Fourier functions, the behavior of PDEs with other sets of functions can be approximated to a certain extent. The final benefit is the mature ecosystem around these functions which include fast algorithms for the Fourier transform and even numerical approaches for solving known PDEs like the previously mentioned spectral

method. In summary the generated data consists of features and labels which are Fourier functions implicitly defining the relationship enforced by a PDE and scenario. After establishing the kind of functions to be used in dataset generation, the process can proceed. There are 4 steps involved in the data generation:

1. Scenario and PDE Determination: The first step of data generation is determining the scenario related to the PDE or governing equations. First, the PDE to be modeled is determined based on the goals of the dataset. Then, one or more of the parameters is chosen to predict the solution. The chosen parameters will be called the input functions and the solution will be called output functions from here on. The second part of the scenario is the domain or more simply the physical space occupied by the system to be modeled. The domain will be used to compute the function values in relation to the physical space from coefficients of Fourier functions.

2. Parameter Determination: The second step is determining all parameters other than that input parameter based on the scenario and governing equation. These parameters may be coefficients such as material properties like density or viscosity, or forcing terms which model external influence on the system like a heat source in the case of the heat equation. Depending on the parameters, solutions of PDEs may behave very differently, such as the appearance of discontinuities in the solution to low viscosity Burgers' equation. Because of this, the choice of parameters is guided by what the dataset seeks to do.

3. Random Coefficient Generation: The third step of data generation is randomly generating the solutions for the chosen equation. Generating random functions in the space of Fourier functions exploits the fact that the coefficients characterize the function completely. By randomly assigning coefficients c_k, many functions can be generated randomly with very little cost. Since the coefficients need to be complex numbers as in equation (2.1), both real and imaginary components are generated independently by assigning a random value to each component for each wave number k. They are then put together again into complex numbers.

   Since only real functions are of interest in this study, the generation cost can be approximately halved. This is because for real functions the coefficients for negative wave numbers k are complex conjugate of the positive wave numbers.

This means that once the positive coefficients are generated, one only needs to compute their complex conjugate and concatenate the result with the coefficients of positive wave numbers. For dimensions higher than one, a simpler approach is used. The coefficients are generated for all wave numbers including the negative ones. The inverse Fourier transform is computed and this results in complex functions. The real components of these functions are kept and the Fourier transform is applied to get the coefficients of the real functions. Finally, these generated coefficients then be used with the basis functions as input functions.

4. Forcing Term Computation: Finally, in order to ensure that the generated solution and chosen parameters satisfy the equation, the forcing term is computed as the residual of the equation of interest with the parameters that was previously determined. This computation is done using the spectral method.

5. Function Value and Noise Computation: The generated solution and forcing functions are labeled as input and output functions. The values of both functions in the domain can then be computed using the scenario determined in the first step. Once all coefficients are generated, the function values are computed with an inverse Fourier transform. The real component of the function values are retained, and the imaginary component are zeroed out. Noise is added to the function values here as needed. The processed function values are then converted back into coefficients using a Fourier transform. This processing is necessary to ensure that the coefficients are only describing the real function.

These four steps are the general processes involved in generating datasets for this study. Further specifics of the generation process of each dataset is explained in their respective subsections.

4.1.1 Data Generation: Anti-derivative

The first dataset is a simple one dimensional derivative. This was chosen as a simple proof of concept of the ability to solve a differential equation. The equation is related to many real-world problems such as acceleration and speed. One can imagine a train in an ideal world where acceleration is directly translated into speed. When the train accelerates at time t by some amount a, we can expect the train to have some speed u. In this ideal world, the relationship between speed and acceleration can be modeled

with a simple differential equation (4.1). This scenario is found in many real systems albeit often with many more details such as different components of acceleration from friction, drag, gravity, and other factors. As previously mentioned in section 4.1, both velocity u and acceleration a are modeled with Fourier series in equations (4.2) and (4.3) respectively.

$$\frac{\mathrm{d}u(t)}{\mathrm{d}t} = a(t) \tag{4.1}$$

$$u(t) = \sum_k \hat{u}_k e^{2\pi i k t} \tag{4.2}$$

$$a(t) = \sum_k \hat{a}_k e^{2\pi i k t} \tag{4.3}$$

The domain of the scenario is a two-hour time window. This number was chosen because it is around the ideal length of travel time on high speed rail in comparison to air travel and car travel (Givoni, 2006; Nash, 1991; X. Wang & Zhang, 2019). This is the first step in generating this dataset.

In the second step, as the derivative equation (4.1) does not contain any parameters other than the acceleration which is the input parameter, there are no other parameters to determine. Therefore, the data generation process proceeds to generating coefficients for the speed functions $\hat{u}$. The coefficients are assigned randomly from a Gaussian distribution with a mean of zero and standard deviation of one. This choice was made such that most wave numbers will have a coefficient of close to zero leaving a sparse set of wave numbers to mostly affect the resulting function. In total, 5000 unique functions are generated with 100 complex coefficients each.

In the third step, the output function coefficients are computed. To find the relation between $\hat{u}_k$ and $\hat{a}_k$, we need to find substitutes for each term in equation (4.1). To do this, we take the derivative of equation (4.2) which result in equation (4.4). Using this we can substitute the terms in equation (4.1) with equations (4.3) and (4.4) giving equation (4.5). Finally, after some algebraic manipulation we obtain the relationship between the input a^* and output function u^* in terms of their coefficients in equation (4.6). One also needs to choose the integration constant $\hat{u}_0$ because at $k = 0$

equation (4.6) becomes a division by zero.

$$\frac{\mathrm{d}u(x)}{\mathrm{d}x} = \sum_k \hat{u}_k \times (2\pi ik)\, e^{2\pi ikx} \tag{4.4}$$

$$\sum_k \hat{u}_k \times (2\pi ik)\, e^{2\pi ikx} = \sum_k \hat{a}_k e^{2\pi ikx} \tag{4.5}$$

$$\hat{u}_k = \hat{a}_k / (2\pi ik) \tag{4.6}$$

In the final step, using randomly generated values of $\hat{a}_k$, the corresponding values of $\hat{u}_k$ are computed with equation (4.6). These coefficients are then used to compute the function values inside the domain. The two-hour time window is represented by a grid of 500 discrete points. With the coefficients and evaluation points ready, the function values are computed using equations (4.2) and (4.3). Next, noise is added to the function values in order to motivate models learning on the dataset to generalize on noise. To also allow evaluation of how well the model performs with different levels of noise, the samples are duplicated into three copies for each high, medium and low noise levels. The function values of each copy is perturbed with noise from a Gaussian distribution with zero mean and standard deviation of some percentage of the average function value standard deviation. The percentages of each high, medium, and low noise levels are 5, 10, and 50 percent. The perturbed function values are then transformed back into their coefficients. An example generated function and its different perturbed versions is shown in figure 4.1a. The horizontal axis indicates time which is displayed in units of hours. The vertical axis indicates velocity in abstract units.

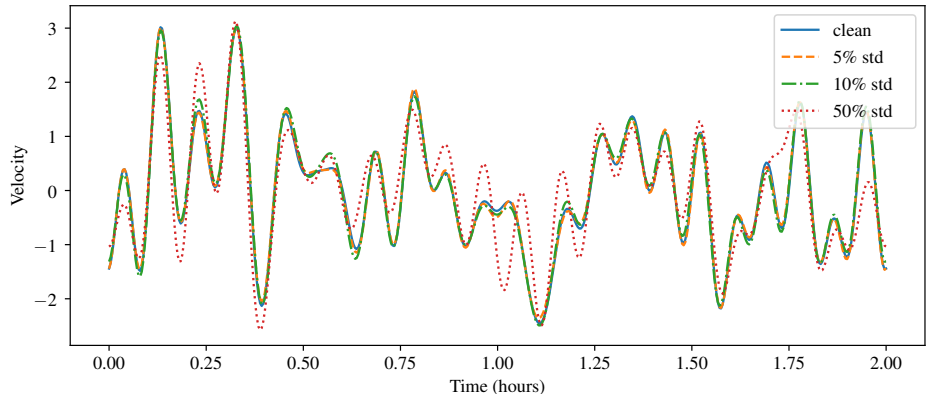

(a)

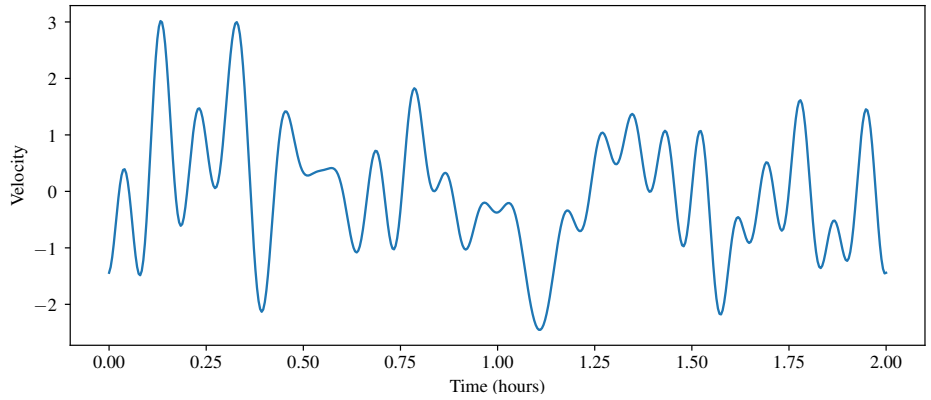

(b)

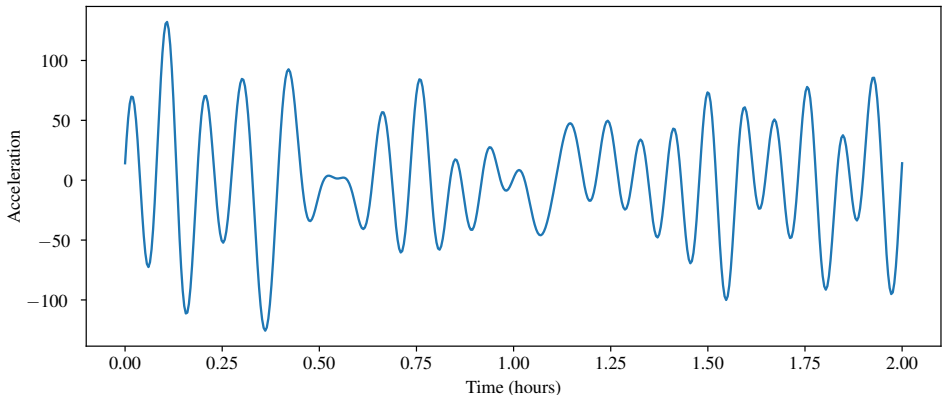

(c)

Figure 4.1: (a) A generated function with no noise (clean), low noise level (5%), medium noise level (10%), and high noise levels (50%). (b) Antiderivative function with no noise. (c) Derivative function with no noise.

4.1.2 Data Generation: Burgers' Equation

The second dataset generated in this study concerns the Burgers' equation. This equation has been used to model a variety of cases including fluid dynamics, traffic flow, and, shock waves (Bec & Khanin, 2007; Bonkile et al., 2018; Jameson, 2007; Orlandi, 2000). This equation is also used as a base problem for testing the effectivity of numerical methods in solving non-linear PDEs (Banks et al., 2012; Barter, 2008; Bonkile et al., 2018; Tabatabaei et al., 2007). The nonlinear term in the equation creates steep gradients and even shock waves which are discontinuous with low viscosity conditions. These challenges test the stability of numerical solvers. This is the scenario and reason for the choice of this PDE. To control the viscosity and therefore the steepness of gradients, the formulation of the Burgers' equation considered in this study is the forced viscous Burgers' equation in one dimension. For a velocity of $u(x,t)$, viscosity of ν, and forcing term of $f(x,t)$, the formulation of the forced Burgers' equation is shown in equation (4.7).

$$\frac{\partial u}{\partial t} + u\frac{\partial u}{\partial x} - \nu\frac{\partial^2 u}{\partial x^2} = f \tag{4.7}$$

The domain of we consider here is based on an exact solution of the equation. This is done so that the learned solver model can be tested on the exact solution. There are a number of sources in literature on the exact solution of the Burgers' equation (Benton & Platzman, 1972; Wazwaz, 2010; Wood, 2006). In this study, we use a specific solution by Wood (2006) which can be seen in equation (4.8). This solution is periodic in space but not in time. Therefore, the domain in space will be based on the spatial periodicity of the exact solution which is two. As such, the space domain spans from 0 to 2. The time domain, on the other hand, is chosen to span from 0 to 10 such that enough details of the solution is included.

$$u(x,t) = \frac{2\nu\pi e^{-\pi^2\nu t}\sin(\pi x)}{a + e^{-\pi^2\nu t}\cos(\pi x)} \tag{4.8}$$

Continuing to the second step, the parameters involved in equation (4.7) are the viscosity ν and the forcing term f. Since the forcing term is dependent on the solution in this step, the only parameter to determine is the viscosity. We choose three constant viscosity values which are 0.1, 0.01, and 0.0. These values are chosen so that a variety of behaviors are represented in the dataset from viscous to inviscid flow.

After this, in the third step, the solution functions u are generated with 20 modes in time and 20 in space and 500 unique function samples for each viscosity value. In total 1500 unique solution functions are generated.

As for the forcing term, it is computed using equation (4.7). The solution field u and forcing term f are modeled with Fourier series in equations (4.9) and (4.10) where k is a vector of spatial and temporal wave number such that k_t is the temporal wave number and k_x is the spatial wave number.

$$u(x,t) = \sum_{k_x}\sum_{k_t} \hat{u}_k e^{2\pi i(k_x x + k_t t)} \tag{4.9}$$

$$f(x,t) = \sum_{k_x}\sum_{k_t} \hat{f}_k e^{2\pi i(k_x x + k_t t)} \tag{4.10}$$

Substituting the terms in equation (4.7) with the respective Fourier series, we get the equation equation (4.12). A problem one notices is the nonlinear term $u\frac{\partial u}{\partial x}$. A naive approach would multiply all wave numbers terms with each other.

$$u\frac{\partial u}{\partial x} = \left(\sum_{k_x}\sum_{k_t} \hat{u}_k e^{2\pi i(k_x x + k_t t)}\right) \times \left(\sum_{k_x}\sum_{k_t} (2\pi i k_x)\hat{u}_k e^{2\pi i(k_x x + k_t t)}\right) \tag{4.11}$$

This is computationally expensive operation with N^2 multiplications (Larios, 2021; Orszag, 1972; Roberts & Bowman, 2011; Shen, 2011). To avoid this complexity, the term is first reformulated into $\frac{\partial}{\partial x}\left(u^2/2\right)$. Then to avoid aliasing, the coefficients are padded with 50% zeros such that the padded coefficients are 3/2 times the size of the original (Larios, 2021; Orszag, 1971). Then we use the padded coefficients to compute the function values in the physical domain using the inverse transform. And then, the point wise squaring operation is performed and transform the results back to spectral domain. The resulting coefficients are then trimmed back to their original size before padding. Finally, we multiply the resulting coefficients $\imath\hat{u}_k$ by the derivative constants. This operation is much more efficient with only $1.5N$ multiplications. This is still more efficient than the naive approach even after taking into account the transforms involved adds $O(2 \times 1.5Nln(1.5N))$ operations if using a Fast Fourier Transform algorithm.

Putting all the above together, results in equation (4.12).

$$\begin{aligned}\sum_{k_x}\sum_{k_t}\hat{f}_k e^{2\pi i(k_x x+k_t t)} =& \sum_{k_x}\sum_{k_t}(2\pi i k_t)\hat{u}_k e^{2\pi i(k_x x+k_t t)} \\ &+\sum_{k_x}\sum_{k_t}(2\pi i k_x)\iota\hat{u}u_k e^{2\pi i(k_x x+k_t t)} \\ &-\nu\sum_{k_x}\sum_{k_t}(2\pi i k_x)^2\hat{u}_k e^{2\pi i(k_x x+k_t t)}\end{aligned} \tag{4.12}$$

$$\sum_{k_x}\sum_{k_t}\hat{f}_k = \sum_{k_x}\sum_{k_t}(2\pi i k_t)\hat{u}_k + (2\pi i k_x)\iota\hat{u}u_k - \nu(2\pi i k_x)^2\hat{u}_k \tag{4.13}$$

$$\hat{f}_k = (2\pi i k_t)\hat{u}_k + (2\pi i k_x)\iota\hat{u}u_k - \nu(2\pi i k_x)^2\hat{u}_k \tag{4.14}$$

After simplifying the equation, we get the coefficients as in equation (4.14). Using this equation, the exact forcing term corresponding to the randomly generated solution can be computed with relatively low cost. Finally, the function values of both the solutions and forcing terms are perturbed by adding Gaussian noise with a mean of zero and standard deviation of 10% of the function value standard deviation to the values of the inverse transform. The perturbed coefficients are then recomputed from the sum and the final perturbed functions are obtained.

4.2 Data Retrieval

The second data acquisition approach retrieves data of a from an external source. This approach downloads the external data to a local machine. In this study, the specific dataset that will be used is the ERA5 dataset from the European Center for Medium-range Weather Forecast (ECMWF). Specifically, the ERA5 dataset is a reanalysis which means it combines observational data from all over the world in order to present a more complete picture of the weather system. This combination process, named 4D variational data assimilation, takes into account the physics known to be involved in the system. As an example weather station data which take measurements such as wind speed, humidity, and temperature of the immediate surroundings of the weather station is very limited in giving a broader picture of weather over a larger area. Even technologies like earth observations satellites are limited to what they can observe at any single point in time as most cannot see the entirety of the earth's

surface at once. The ERA5 dataset specifically, assimilates previous forecasts with observational data every 12 hours. The ERA5 reanalysis is available at the following url (https://cds.climate.copernicus.eu/datasets/reanalysis-era5-single-levels).

The original dataset made available by ECMWF has a grid size of 0.25° by 0.25° in latitude and longitude for atmospheric data. Data of oceanic waves are also available at a coarser grid size of 0.5° by 0.5°. However, we will use a cloud optimized version called WeatherBench2 that is easier to retrieve (Rasp et al., 2023). This is because the data is available in several more grid sizes such as 1.5°. In addition, the data can be readily downloaded to a local machine without waiting for further processing on the server. The guide for working with the dataset is available at (https://weatherbench2.readthedocs.io/en/latest/data-guide.html). In our specific case, we use the version labeled `1959-2023_01_10-6h-64x32_equiangular_conservative.zarr`. This dataset spans from year 1959 to 2023 with a grid size of 5.625° or resolution of 64 by 32 which spans from $-87.19°$ to 87.19° in latitude and 0.0° to 354.4° in longitude. The dataset is also downsampled to 6 hour intervals that starts at midnight UTC January 1959 1st and ends at 18:00 UTC January 10th 2023.

While the original data provided by ECMWF is available in NetCDF or GRIB, the WeatherBench2 version is provided using the Zarr format in a Google Cloud Storage Bucket. This setup allows the use of libraries that support the Zarr format to access the dataset remotely. The particular library we use is called *Xarray* version `2024.9.0` (Hoyer & Hamman, 2017; Hoyer et al., 2024). Accessing the remote dataset is done as shown in figure 4.2. In order to ensure access is granted, the storage option token is set to anon so that the method uses the anonymous only public access mode of authentication ("GCSFS — GCSFs 2023.12.2post1+1.G8e500c6.Dirty Documentation," n.d.).

```
1  import xarray as xr
2  xr.open_zarr(
3      "DATASET_ADDRESS",
4      storage_options = {"token": "anon"},
5  )
```

Figure 4.2: Example of using Xarray to access a publicly accessible Zarr dataset hosted on Google Cloud Storage Bucket.

The dataset includes 62 variables with some variables also spanning 13 discrete vertical levels in the atmosphere. For our use, we will only be using the 2-meter temperature of the atmosphere. This is the air temperature 2 meters above the surface be it land, sea, or inland water. This variable is in units of kelvin. The values of this variable is obtained by interpolating between the model values at the surface and the lowest model vertical level. We also limit the time range to .... An example of the data that was retrieved can be seen in .

4.3 Design of Computational Model

In this section, we will discuss the design of the computational model that is proposed in this work. An illustration of the computational model is show in figure 4.3.

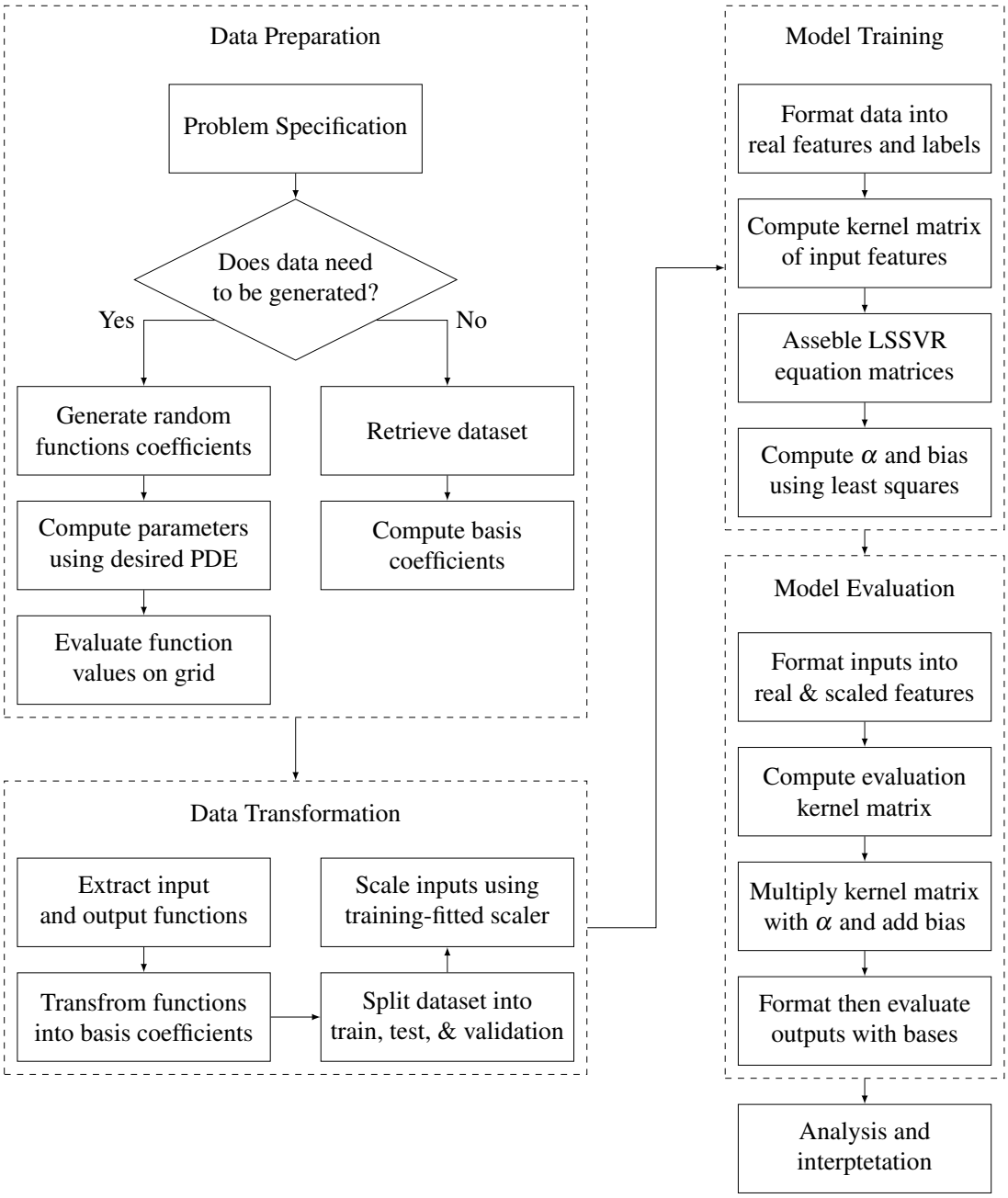

Figure 4.3: Computational Model of SpectralSVR.

The computational model is divided into four large phases. The processes within these phases are based on the broad outcomes of the phase. The phases themselves are data preparation, data transformation, model training, and model evaluation. Each phase is composed of processes that together works toward the output of the larger process. At the end, a final process of analysis and interpretation is carried out.

4.3.1 Data Preparation

The data preparation phase starts off the computation by preparing the data that is to be used in this study. This phase starts with specifying the problem to be solved. This translates to the dataset that will be used to represent these problems. The first type of dataset is generated based on a known governing equation or PDE. Using said equation, the goal is to generate pairs of functions that are related to each other by the equation. In the next process, generally, the solution function is first generated randomly. This is done by generating random numbers to use as coefficients of a set of basis functions. Then parameters of the equation is determined, such as term coefficients. Using the generated solution and predetermined parameters, a forcing term can generally be computed to satisfy the equation. Augmentations such as noise can then be added in the final process which is evaluating the function values. These processes result in a generated dataset. To verify the generation method and any models trained on the generated data one can use exact analytical solutions of the governing equations.

The second type of dataset is retrieved from an external source. The data source is first identified, in our case it is the WeatherBench 2 collection of datasets. The specific dataset from the collection of different dataset versions is first determined. The dataset is available in the *Zarr* format. And then, we determine the filters for the portions of the dataset we are interested in. Once the dataset and filters are determined, the retrieval process starts by accessing the dataset using the *Xarray* library (Hoyer & Hamman, 2017; Hoyer et al., 2024). The filters are applied as in .... Finally, the filtered version is stored locally. The local dataset is also stored in the *Zarr* format.

4.3.2 Data Transformation

The second phase of the computational model transforms the data that has been prepared into a form that can be used with the proposed model. In this study, there are two ways a dataset can be used. The first and simplest way is to predict the solution function from the forcing term for a given set of PDE parameters. In this case, the input function is the forcing term. In other words, the input function is the predictor or independent variable that will be used to predict the solution function. As such, the output function is the solution function. The antiderivative dataset is used in this way. The derivative, which represents the acceleration function, is used to predict the

velocity function. Which means that the input function is the acceleration function and the output function is the velocity function. The second use of a dataset depends on whether it can be interpreted as a mapping of a previous function to the next function. In other words, a series of functions related to the previous function as a sum of the previous function and a perturbation. A commonly used form of this are time series. Generally, a time series can be represented as equation (4.15). This function describes the evolution of function f as a sum of some initial state f^0 and perturbation which is its rate of change $\frac{\mathrm{d}f}{\mathrm{d}t}$ at a point in time close to the current time multiplied by the time step δt.

$$f^{t+1} = f^t + \delta t \times \frac{\mathrm{d}f}{\mathrm{d}t} \tag{4.15}$$

In this case the previous function and any other independent variables like the forcing term involved in the time derivative $\frac{\mathrm{d}f}{\mathrm{d}t}$ is used to predict the perturbation which is the time derivative itself. It would mean that each sample function in the data would need to at least have two dimensions. This is because one dimension represents the evolution of the function over time, while the other dimensions define the spatial domain where the function's values are computed at each time step. This condition is true for both the Burgers' equation dataset and the WeatherBench 2 collection of ERA5 datasets. First, the Burgers' equation dataset, while is also able to be used in the first way as a mapping between the forcing term and the solution, one of the traditional ways of solving it is using the method of lines in conjunction with another method such as the finite differences method or the spectral method. In both of these, the Burgers' equation is formulated as an initial value problem, using the finite differences to computing the time derivative. The method of lines approach in one of its forms is equal to equation (4.15) (Sadiku & Obiozor, 2000; Schiesser, 2012). As such the Burgers' equation dataset can also be used in this way. In this case, algebraic manipulation of equation (4.7) results in the time derivative of the solution as in equation (4.16).

$$\frac{\partial u}{\partial t} = f - u\frac{\partial u}{\partial x} + \nu\frac{\partial^2 u}{\partial x^2} \tag{4.16}$$

As can be seen, the time derivative is expressed in terms of the solution function, the forcing term and any other partial derivatives. Because of this, it means we can train the model to learn the relationship between the solution function combined with the forcing term and the time derivative. Putting this together with equation (4.15), it is possible to

predict the solution function in a future time based on the current solution function and forcing term. The input functions in this case are both the value of the solution function and the forcing term at the current time step. The output function is the time derivative which is computed by rearranging equation (4.15) resulting in equation (4.17).

$$\frac{\mathrm{d}f}{\mathrm{d}t} = \frac{f^{t+1} - f^{t}}{\delta t} \tag{4.17}$$

Perhaps in a more obvious manner, the same is also applied to the WeatherBench 2 collection of ERA5 datasets. The 2-meter temperature is a series of snapshots in time of the distribution of temperature all over the world at 2 meters above the surface. The input function in this case is the temperature distribution at the current time step. The output function is the time derivative of the temperature distribution computed using equation (4.17).

The input and output functions are then transformed into basis coefficients using the Fourier transform. Once the coefficients are computed, the input and output sample pairs are split into train, test, and validation subsets. For the first type of input and output function pair, since the samples are independent of each other, a random sampling of the dataset without replacement is done to select the samples for each subset. For the second type of input and output function pairs, if there are multiple samples of functions as in the Burgers' equation dataset, the same process with random sampling is followed. On the other hand, if only one function sample is available, such as the WeatherBench 2 dataset, an issue that arises is the fact that the samples are dependent on one another. This is because a previous time step influences the next time step. This is a problem for generalizing the learned model, since random sampling would lead to the model learning information in the future of the testing subset (Kapoor & Narayanan, 2023; Kaufman et al., 2012). As such, the portioning of the dataset is done by dividing the sample into different sections of the function in time.

Finally, the data is scaled. This is done because of how support vector machines require scaling for inputs in order to perform well with certain hyperparameters such as the RBF kernel (Ben-Hur & Weston, 2010). For our case we use standard scaling based on the inputs of the training subset. This approach transforms the dataset by manipulating the distribution characteristics of the dataset (Ahsan et al., 2021). Specifically, the standard deviation σ and mean x_0 of the dataset values x are processed

such that the resulting values have a mean of 0 and standard deviation of 1. The function shown in equation (4.18) represents how each sample is processed with respect to the standard deviation σ and mean x_0 of each feature.

$$z(x;\sigma,x_0) = \frac{x - x_0}{\sigma} \tag{4.18}$$

The scaling is important for the RBF kernel specifically due to the fact that the kernel utilize a scale parameter. This parameter affects how scale of values influence the kernel. Another and perhaps more general benefit of scaling is the uniformity it enforces across features. This is useful because all feature weigh the outcome equally. In our use case, this equality is a reflection of what the data actually represents. Each feature which is a discretized value or its coefficient representation has equal value to any other feature. No point or coefficient is any more or less value compared to another point or coefficient.

The scaling is applied to input functions only because scaling of the outputs does not affect the performance of the model (Ben-Hur & Weston, 2010). To also prevent information leakage across training and testing sets, the mean and standard deviation of each feature is computed using the training subset only. Once the parameter values are obtained, all input function samples in the dataset are transformed into their scaled versions. This means that the distribution for the testing and validation sets may be outside the target standard deviation and mean.

4.3.3 Model Training

Once the data has been preprocessed, the model is trained using pairs of training features and labels. The training phase is separated into four processes. First, the preprocessed input and output function representation need to be real numbers. This is because the LSSVR model was made to work with real numbers. Any complex values such as Fourier coefficients are represented as flattened pairs of the real and imaginary components of complex values.

The training can proceed to solve equation (2.10). As the original LSSVR equation was made for regression of a single value of $\mathbf{y}$, we constructed an extended the original equation in order to train multiple regression models to predict each coefficient in an output function sample. The assumption of this extension is that the inputs and model

hyperparameters such as kernels and the regularization constant C are the same across individual regressors. Therefore, it follows that the solution vector and target vector can both be transformed into their matrix form with each column representing the individual regressor which results in equation (4.19). This vectorized version is equal to m separate instances of equation (2.10). In essence, instead of a vector of scalar sample output values and a vector of model parameters, the extended equation consists of a matrix of rows of vector output values and a matrix of model parameters with each column representing the separate model for each output and row representing the Lagrange multipliers for each sample. The procedure to solve equation (4.19) adjusts algorithm 1 for the extra dimension spanning the multiple outputs of size m.

$$\begin{bmatrix} 0 & \mathbf{1}_n^\intercal \\ \mathbf{1}_n & \Omega + \frac{I}{C} \end{bmatrix} \begin{bmatrix} b_0 & \cdots & b_m \\ \alpha_0 & \cdots & \alpha_m \end{bmatrix} = \begin{bmatrix} 0 & \cdots & 0 \\ \mathbf{y}_0 & \cdots & \mathbf{y}_m \end{bmatrix} \tag{4.19}$$

Second, as the training process of an LSSVR described in requires constructing the first matrix on the left-hand side and the matrix on the right-hand side, each component of the matrices themselves will also need to be constructed. The kernel matrix Ω is first constructed by computing the kernel values between each sample input with every other sample input. If the training set has n samples, then the resulting kernel matrix would be of size n by n. Third, using the inputs $\mathbf{X}$, outputs $\mathbf{y}$, predetermined regularization constant C, and the obtained kernel matrix Ω, equation (4.19) is assembled. Finally, the matrix of learned parameters α and $\mathbf{b}$, which are the Lagrange multipliers and bias respectively, are solved for using a linear equation solver such as a matrix Moore-Penrose inverse or linear least squares solver.

Next, the selection of hyperparameters is done to optimize the model further. As previously mentioned, the hyperparameters are the regularization constant C and kernel functions including the kernel function parameters.

4.3.4 Model Evaluation

The fourth phase of the computational model is the evaluation of the learned model. This phase starts with formatting the inputs. If the inputs aren't scaled yet, then it is scaled using the scaler fitted on the training set. This is the case for new data such as new measurements or an analytical solution of the learned PDE. Once the inputs that is to be evaluated is scaled in the same way as the training inputs, the model can predict

the corresponding outputs.

The procedure to compute the predicted outputs follows algorithm 2. This leads to the second process which is computing the kernel matrix between the training input features $\mathbf{X}$ and the evaluation input features $\mathbf{U}$. The matrix is constructed as the kernel value between each evaluation sample feature and every training sample feature. For p evaluation samples and n training samples, this results in a kernel matrix Ω with a shape of p rows and n columns.

In the third process, the constructed kernel matrix is then multiplied with the matrix of learned Lagrange multipliers α. The multiplication is the matrix multiplication process. Then, the bias vector is added to each row to produce the final predicted outputs $\mathbf{v}$. This process is represented by equation (4.20).

$$\mathbf{v} = \Omega\alpha + \mathbf{1b} \tag{4.20}$$

The fourth process is concerned with the fact that the predicted output $\mathbf{v}$ is a matrix of real numbers. The LSSVR output needs to be formatted before it can be used in the proposed model. This is done by converting the outputs into the same format as the training labels. As we use the Fourier basis, the model output is converted back into a matrix of complex numbers using the inverse of the first process during training. Finally, these predicted Fourier basis coefficients can be used to evaluate the predicted functions themselves.

4.4 Implementation of Computational Model

This section discusses the implementation of modeling and approximation of PDEs using LSSVR. Using the computational model design in section 4.3, the computational model is implemented as a library using the Python programming language. The development process itself is based on the iterative development model as mentioned in section 3.4. In this section, the output iterative processes are consolidated and explained together.

4.4.1 Analysis

The aim of any program that is developed in this study is to model the relationship between functions defined by a partial differential equation or other operators and governing equations. Since the potential subject of modeling can be wide-ranging, the software product that will be developed is a library. This is done so that the tools and proposed model that is developed will be able to be used with a variety of PDEs. With this in mind, the software must also be performant and compatible with the larger machine learning and scientific computing community.

To demonstrate the use and capability of the software, three case studies are chosen to represent the variety of PDEs. The first case study is the antiderivative equation. This simple case is chosen as a proof of concept to show that the proposed model works in the most simple case. The second case study, which is the Burgers' equation, adds a level of complexity because of the nonlinearity involved with the solution function. The third case study, which is the ERA5 weather dataset, was chosen to show how the model performs on data with real world observations incorporated into it. This dataset also presents a challenge because of the uncertainties involved with weather simulation (Herrera et al., 2017). These datasets are discussed in sections 4.1 and 4.2.

In addition, the software product is developed within certain limitations. The limitations are:

1. The operating and implementation language of the library is Python.
2. The library is to be used in user code
3. The library depends on other libraries including the following core dependencies Pytorch, Numpy, Xarray, Zarr, Pandas, and tqdm.

4.4.2 Design

In this subsection, the architectural design of the software product is explained. The architecture consists of modules with similar concerns. This was chosen because of the intuition built by the use of other libraries with a similar architecture. The broad aim of modeling PDEs with LSSVR and basis functions coefficients can be separated into smaller concerns of data, model, and basis functions. Each of these concerns are addressed by a corresponding module. The explanation of each module are as follows:

1. Utilities

   This module provides basic tools that are used across the entire library. The utilities this module needs to provide include scaling, conversion between real and complex representations of matrices, resizing coefficient tensors, and adaptors for or the traditional ordinary differential equation solvers. Scaling functionality is used for inputs into the support vector machines. And as previously mentioned, since LSSVR only works with real numbers, the tools for converting between complex and their real number representations is also necessary. Another useful tool for working with basis coefficients is a way to resize the coefficients in terms of how many basis functions is desired. An example of the usage is downsizing Fourier coefficients from 12 to 8 modes. The last utility mentioned here provides the ability to solve ordinary differential equations. This utility is useful for generating data for certain types of PDEs such as the Burgers' equation.

2. Basis Functions

   As the proposed model will learn the relationships defined by PDEs within the spectral domain, a large proportion of the computation will also concern the use of the basis functions themselves. The module will define the functionality and data structure that is expected to be used when working with basis functions in this library. First and foremost, the central function of this module is to store and facilitate the connection between the coefficients in the spectral domain and their values in the physical domain. This is dependent on the basis functions used. For the Fourier basis that we use in this study, this means that the transformations are the discrete Fourier transform and the discrete inverse Fourier transform. Other than this core functionality, information on the characteristics of the coefficients such as the number of modes, in other words basis functions, should also be provided by this module. In addition, other functionality included in this module are visualization of coefficients in physical space, generation of random functions, time dependent & complex/real coefficients, noise perturbation of functions, and differential operators.

3. Model

   The proposed SpectralSVR model is implemented in this module. As the

proposed model essentially wraps a support vector regression model in such a way that it can process coefficients, this module will house the SpectralSVR wrapper itself and the LSSVR variant of support vector regression that is used in this study. The SpectralSVR wrapper must provide three core pieces of functionality. First, it must translate complex input and output samples into their real representations. This applies to both training and evaluation. Second, in addition to predicting the coefficients during evaluation, the wrapper should also be able to predict the function values themselves for any given set of point coordinates. This is important for quick evaluations of a predicted function at an arbitrary point. The third functionality is inverse input function search for a given output. This is useful for inverse problems where the parameters are unknown, but the solution is partially known. Aside from the core functionality, a complementary functionality is testing for the learned model.

The model module also implements the LSSVR model. This implementation provides two main functionalities. The first is training the LSSVR model with some given model hyperparameters such as the regularization constant and kernel. The second functionality is the evaluation of the learned model. Both functionalities allow for multiple output regression. This is required to learn the mappings for many coefficients at once. Other functionality provided by the implementation include interpretability functions and model serialization for saving and loading the learned model to disk.

4. Problems

This module provides the functionality concerned with generating data. Two out of the three datasets in this study are generated with this module. In general this module provides two pieces of functionality. The first is generation of the data itself. This functionality generates at least two sets of functions that are related to each other by the chosen PDE. The generation is based on at least two parameters which are the number of samples to generate and the number of modes or basis functions to generate the coefficients for. The second functionality provided by this module is the residual based on the chosen PDE. This is useful to verify if any set of functions comply with the PDE. For example, the residual may be used to verify the generated data. Another use is to grade the predictions by the learned model.

The design presented here is the product of multiple iterations that started with building the core model and then the basis functions and finally the data. Throughout the iterations, the utilities were also added to alleviate the need for general tools.

4.4.3 Implementation

The design in section 4.4.2 is implemented within the same iterative loop. As such, the feedback from tests is immediate, and any fixes can be implemented quickly. The implementation is done using the Python language and a number of Python libraries. To facilitate the management of dependencies, the implementation makes use of the package management tool Poetry (Eustace, 2024). In addition, the Python version is managed using the tool pyenv. The implementation process starts with installation of the required dependencies. The dependencies are specified in the `pyproject.toml` as shown in figure 4.4.

```
...
[tool.poetry.dependencies]
python = "^3.10.6"
numpy = "^1.24.0"
tqdm = "^4.65.0"
jaxtyping = "^0.2.20"
pandas = "^2.2.2"
torchmetrics = "^1.4.2"
scikit-learn = "^1.5.0"
matplotlib = "^3.9.0"
torch = {version = "^2.4.1+cu124", source = "pytorch-gpu"}
torchvision = {version = "^0.19.1+cu124", source = "pytorch-gpu"}
torchaudio = {version = "^2.4.1+cu124", source = "pytorch-gpu"}
ray = {extras = ["tune"], version = "^2.37.0"}
hyperopt = "^0.2.7"
ipywidgets = "^8.1.5"
torchdiffeq = "^0.2.4"
xarray = "^2024.10.0"
zarr = "^2.18.3"
gcsfs = "^2024.10.0"

[[tool.poetry.source]]
name = "pytorch-gpu"
url = "https://download.pytorch.org/whl/cu124"
priority = "explicit"

[build-system]
requires = ["poetry-core"]
build-backend = "poetry.core.masonry.api"
```

Figure 4.4: Contents of pyproject.toml configuration file that define the dependencies using Poetry.

After ensuring that the correct version of python is being used with pyenv, the dependencies specified in the `pyproject.toml` file can be installed using the shell command `poetry install`. At the end of each iteration, the dependencies are subject to change depending on whether any new ones are needed or old dependencies can be removed.

In the following, we will discuss the implementation of each module and how the phases of computational model relates to each implemented functionality. The base data structure that is used in the implementation is the Pytorch Tensor (Ansel et al., 2024). Tensors are a generalization of scalars and array-like structures such as vectors and matrices. This is essential since many computations that is done in the proposed

model are based on matrices and higher dimensional arrays. Pytorch Tensors allow the elements to be of different data types such as floating point numbers of different precision or even complex numbers. In addition to basic operations for working with the Tensors such as matrix multiplications, Pytorch also provides many algorithms for use when working with Tensors such as linear equation solvers or the Fast Fourier Transform. Another reason for choosing to use Pytorch is the ability to parallelize computation using specialized processors such as GPUs. Lastly, Pytorch is widely used in the machine learning community which reflects on its reliability, wealth of community knowledge and support, and active development.

Utilities

The utilities module provide common tools that are used when working with the developed software. First, because the basis function used in this study is the Fourier basis, a large proportion of concern is the storage of Fourier basis coefficients. The Fourier series representation that is used in this study is the complex representation as show in equation (1.2). However, as previously mentioned, least squares support vector machines is constructed to work with real numbers. In order for LSSVR to learn the relationship between complex numbers, a representation of complex numbers in terms of real numbers is necessary. Since sample features and labels for LSSVR need to be flattened into one dimension which result in a matrix with rows of samples, the representation of complex numbers using real numbers can be done after features and labels have been flattened. An example of such a matrix of two samples with four features each can be seen in equation (4.21). To represent the complex number features as real numbers, once can simply split a single complex number into two real numbers. When this is done to the entire matrix of complex numbers, the result is equation (4.22).

$$\begin{bmatrix} -1.03+0i & -0.52+0.39i & -0.54+0i & -0.52-0.39i \\ -0.85+0i & -0.39+0.19i & 0.87+0i & -0.39-0.19i \end{bmatrix} \tag{4.21}$$

$$\begin{bmatrix} -1.03 & 0 & -0.52 & 0.39 & -0.54 & 0 & -0.52 & -0.39 \\ -0.85 & 0 & -0.39 & 0.19 & 0.87 & 0 & -0.39 & -0.19 \end{bmatrix} \tag{4.22}$$

There are several ways to do this in Pytorch, such as extracting the real and imaginary element components into separate matrices and then interleaving the columns to create the real representation. However, a more performant version can be made by using

built-in functions of the library that directly allows views of complex valued tensors as real tensors and vice versa. The `view_as_real` and `view_as_complex` functions allow the conversion between real and complex representations by representing complex valued tensors by adding a dimension of size two for each component of complex numbers. The resulting implementation can be seen in figure 4.5.

```
1 def to_real_coeff(x: torch.Tensor) -> torch.Tensor:
2     return torch.view_as_real(x).flatten(-2)
3
4 def to_complex_coeff(x: torch.Tensor) -> torch.Tensor:
5   return torch.view_as_complex(
6     x.reshape((*x.shape[:-1], -1, 2))
7   )
```

Figure 4.5: Utility function to convert between complex matrices and the real representations.

Another important utility used on inputs for the proposed SpectralSVR is a scaler. This utility has been implemented in a variety of ways and using different tools. However, as the standard scaling is not provided by Pytorch, we have also implemented our own version. The scaler accepts Pytorch tensors or tuples of tensors of real or complex elements. First, the scaler is implemented as a class that is instantiated. The scaler is then fitted onto the reference data to obtain the standard deviation and mean of each feature. This information is stored as properties of the class. Any complex tensors are converted into their real representations using the functions in figure 4.5. Once the scaler instance is fitted, any set of tensors with the same number of features (columns) and element type (complex or real) can be roughly transformed into a standard deviation of one and mean of zero for every feature. This is done by subtracting the fitted mean of each feature from the elements in the column and then dividing with the feature's standard deviation. The implementation also provides a method to retrieve a scaler fitted on a subset of the original tuple of tensors. Serialization for saving to and loading from disk is also implemented. This is done simply by using the Pytorch save and load functions on the scaler instance itself. For some use cases, an inverse scaling operation to the original standard deviation and mean is also essential. The implementation is simply the reverse of the transformation process where the elements are multiplied by the standard deviation and the mean is the added.

Another group of utility in the module is concerned with managing the number of modes a tensor of coefficients has. First, a function called `resize_modes` accepts a tensor of coefficients and the target number of modes in each dimension. The first dimension is always assumed to represent the different samples. Because of this the target modes will only affect the dimensions after the first. The wave numbers are also assumed to be symmetric about zero such that the highest absolute values of the wave number is in the middle of each dimension. The wave number decreases symmetrically as you move towards the edges of the dimension and reaching the lowest absolute wave number at the edges. This is done to ensure compatibility with the way existing libraries such as Pytorch works with tensors of Fourier coefficients. Because of this, shrinking a tensor of coefficients along a dimension means removing the center of the tensor along that dimension. And expanding to a target number of modes that is larger means that the tensor is padded with zeros in the center along the desired dimension. In addition, the remaining coefficients may be rescaled in order to balance the effect of adding or removing coefficients. The implementation is presented in figures 4.6 and 4.7.

```
for dim, (target_mode, current_mode) in enumerate(
    zip(target_modes, current_modes), 1
):
    device = x.device
    start_range = torch.tensor(
        range((target_mode - 1) // 2 + 1), dtype=torch.int
    ).to(device=device)
    end_range = torch.tensor(
        range(current_mode - target_mode // 2,
          current_mode
        ),
        dtype=torch.int,
    ).to(device=device)

    x_resized = torch.concat(
        (
            x_resized.index_select(dim, start_range),
            x_resized.index_select(dim, end_range),
        ),
        dim,
    )
```

Figure 4.6: Example of shrinking a tensor of samples' coefficients to a target number of modes.

```
for dim, (target_mode, current_mode) in enumerate(
    zip(target_modes, current_modes), 1
):
    device = x.device
    start_range = torch.tensor(
        range((current_mode - 1) // 2 + 1), dtype=torch.int
    ).to(device=device)
    # make sure that end range is empty if
    # the coefficient is only size 1
    end_range = torch.tensor(
        range(current_mode // 2, current_mode)
        if current_mode > 1
        else range(0),
        dtype=torch.int,
    ).to(device=device)
    padding_size = target_mode - current_mode
    modes = list(x_resized.shape)
    modes[dim] = padding_size
    padding = torch.zeros(modes).to(x_resized)

    x_resized = torch.concat(
        (
            x_resized.index_select(dim, start_range),
            padding,
            x_resized.index_select(dim, end_range),
        ),
        dim,
    )
```

Figure 4.7: Example of expanding a tensor of samples' coefficients to a target number of modes.

Next, the second way to manage the size of a tensor along a dimension is to interpolate the current values. The implementation uses simple linear interpolation. This is especially useful for situations such as coefficients that are themselves functions of time. This is a common application such as when solving the initial condition problem of a function in space and time. One might represent the function as a Fourier series with basis as functions of space and coefficients as functions of time. In this case, the coefficients for time values that are not available can be interpolated. The implementation of this is shown in figure 4.8.

```
    index_floor = index_float.floor().to(torch.int)
    index_ceil = index_float.ceil().to(torch.int)
    x_ceil = x.index_select(dim, index_ceil)
    x_floor = x.index_select(dim, index_floor)
    # interpolate coefficients
    index_shape = [1 for _ in range(x_floor.ndim)]
    index_shape[1] = -1
    index_scaler = (
        ((index_float - index_floor) / (
          index_ceil - index_floor
        ))
        .reshape(index_shape)
        .nan_to_num()
    )
    # ynt + scaler * (ynt1 - ynt)
    # (1 - scaler) * ynt + scaler * ynt1
    x_interp = torch.lerp(x_floor, x_ceil, index_scaler.to(x))
```

Figure 4.8: Example of interpolating for indices (floating point indices) between the available ones (intiger indices).

Finally, this module also provides the types and reexports implementations of ordinary differential equation solvers from the torchdiffeq library (R. T. Q. Chen, 2021). The implementation can be seen in figure 4.9.

```python
RHSFuncType = Callable[[torch.Tensor, torch.Tensor],
  torch.Tensor
]
SolverSignatureType = Callable[[
        RHSFuncType, torch.Tensor, torch.Tensor,
    ],
    torch.Tensor
]
MixedRHSFuncType = Callable[[
        torch.Tensor, torch.Tensor, torch.Tensor,
    ],
    torch.Tensor,
]
MixedSolverSignatureType = Callable[
    [MixedRHSFuncType, torch.Tensor, torch.Tensor],
    torch.Tensor,
]

def euler_solver(
    rhs_func: RHSFuncType,
    y0: torch.Tensor,
    t: torch.Tensor,
):
    solution = torch.zeros((len(t), *y0.shape)).to(y0)

    j = 1
    solution[j - 1] = y0
    for t0, t1 in zip(t[:-1], t[1:]):
        dt = t1 - t0
        y = solution[j - 1]
        solution[j] = y + dt * rhs_func(t0, y)
        assert (
            solution.isnan().sum() == 0
        ), f"solver encountered nan at timestep {j} (t={t0})"
        j = j + 1
    return solution

implicit_adams_solver: SolverSignatureType = partial(
    odeint, method="implicit_adams", options={"max_iters": 4}
)  # type: ignore

lsoda_solver: SolverSignatureType = partial(
    odeint, method="scipy_solver", options={"solver": "LSODA"}
)  # type: ignore
```

Figure 4.9: Implementation of ODE solvers and the types.

Basis Functions

This module implements two classes. The first is the base Basis class. The second is a subclass implementing the Fourier basis specifically. These classes provide the functionality needed to have an easier time when working with basis functions and their coefficients. First, the core function of these classes is to provide a way to transition between the spectral domain and the physical domain. This is implemented in the base class by storing the coefficients of sample functions as a class property. The coefficients are assumed to be at least of one function.

```
...
    @staticmethod
    def transform(
        f: torch.Tensor,
        res: TransformResType | None = None,
        periodic: bool = True,
        periods: PeriodsInputType = None,
        allow_fft: bool = True,
    ) -> torch.Tensor:
        if not torch.is_complex(f):
            f = f * (1 + 0j)
        res = transformResType_to_tuple(res, tuple(f.shape[1:]))
        periods = periodsInputType_to_tuple(periods, f.shape[1:])
        # perform 1d transform over every dimension
        F = f
        for cdim in range(1, ndims):
            F = FourierBasis._ndim_transform(
                F,
                dim=cdim,
                func="forward",
                res=res[cdim - 1],
                periodic=periodic,
                period=periods[cdim - 1],
                allow_fft=allow_fft,
            )

        return F
...
```

Figure 4.10: Implementation of forward Fourier transform.

The transitions between the coefficients and functions values are implemented as a function to transform function values to coefficients and an inverse transform function to compute function values from coefficients. The base class enforces this by

defining abstract methods which any subclass will need to implement. The FourierBasis subclass then implements the transform and inverse transform functions specific for transitioning between function values and Fourier basis coefficients. As before, the implementation assumes that the first dimension indexes the samples and the rest represent the coefficient wave numbers. This means that the implementation must allow for multidimensional functions. For the Fourier transform and inverse transform, the multidimensional version is relatively simple to implement. The multidimensional Fourier transform essentially performs the one dimensional Fourier transform along one dimension. And then, using the result to perform the one dimensional Fourier transform along the next dimension. This process is repeated until the last dimension. The implementation of the forward transform is presented in figure 4.10. The inverse transform simply changes the `func` parameter to "inverse".

The Fourier transform along each dimension is done by flattening every other dimension into the sample dimension. This essentially means that the function values are "sliced" along the dimension currently being transformed, and that each "slice" is its own "sample". Mathematically, this is simply due to the matrix multiplication of basis functions along one dimension with every other dimension. The implementation of this is shown in figure 4.11.

```
...
    @staticmethod
    def _ndim_transform(
        f: torch.Tensor,
        dim: int,
        func: Literal["forward", "inverse"],
        res: slice,
        periodic: bool,
        period: float,
        allow_fft: bool,
    ) -> torch.Tensor:
        # flatten so that each extra dimension is
        # treated as a separate "sample"
        # move dimension to transform to the end
        # so that it can stay intact after f is flatened
        f_transposed = f.moveaxis(dim, -1)
        # flatten so that the last dimension is intact
        f_flatened = f_transposed.flatten(0, -2)

        F_flattened = FourierBasis._raw_transform(
            f_flatened,
            func=func,
            res=res,
            periodic=periodic,
            period=period,
            allow_fft=allow_fft,
        )
        # unflatten so that the correct shape is returned
        F_transposed = F_flattened.reshape(
          (*f_transposed.shape[:-1], res.step)
        )
        F = F_transposed.moveaxis(-1, dim)

        return F
...
```

Figure 4.11: Implementation of n-dimensional Fourier transform for a specific dimension.

```
...
    @staticmethod
    def _raw_transform(
        f: torch.Tensor,
        func: Literal["forward", "inverse"],
        res: slice,
        periodic: bool,
        period: float,
        allow_fft: bool,
    ) -> torch.Tensor:
        match func:
            case "forward":
                sign = -1
            case "inverse":
                sign = 1
        mode = f.shape[1]
        domain_starts_at_0 = res.start == 0
        domain_end_equal_to_period = res.stop == period
        can_use_fft = (
            domain_starts_at_0
            and domain_end_equal_to_period
            and periodic
            and allow_fft
        )
        if can_use_fft:
            if func == "forward":
                F = torch.fft.fft(
                  f, dim=1, n=res.step, norm="backward"
                )
            elif func == "inverse":
                F = torch.fft.ifft(
                  f, dim=1, n=res.step, norm="forward"
                )
        else:
            if periodic:
                n = res.start + torch.arange(res.step).to(f)
                n = n / res.step * period
            else:
                n = torch.linspace(
                    res.start, res.stop, res.step
                ).to(f)
            e = FourierBasis.fn(
                n.view(-1, 1),
                mode,
                periods=period,
                constant=sign * 2j * torch.pi,
            )

            F = torch.mm(f, e.T)
        return F
...
```

Figure 4.12: Implementation of the one dimensional Fourier Transform.

The one dimensional Fourier transform itself is implemented as a raw transform function. This function accepts input of a matrix of values to transform, a parameter to indicate the type of transformation (inverse transform or forward transform), the evaluation boundary and number of grid points, whether the evaluation should assume the function is periodic, the size of the function domain, and if the Fast Fourier Transform is allowed to be used. The evaluation boundaries, actual function domain size, whether the function can be assumed to be periodic, and if FFTs is allowed to be used together determine the Discrete Fourier Transform algorithm that is used. The FFT algorithm is used if the folowing are all true: the evaluation starts at zero and ends with the same value as the period, the function can be assumed to be periodic, and FFT is allowed. Otherwise, the transform is computed naively using equations (2.3) and (2.4). The naive approach allows for evaluating function values of coefficients at various grid sizes and evaluation boundaries. This is useful for being able to evaluate at resolutions other than that of the original discretized function or coefficients. One use for this is plotting the function at different parts or resolutions. The relationship with the physical domain means that the boundaries of the domain is important. This is because the function values that will be used may only be valid within certain boundaries. Because of this, the information of physical domain bounds must also be stored. This is done by storing the span of the function in each dimension. The implementation we have gone with doesn't store any other information than the span in each dimension. Because of this, the information would need to be stored outside the Basis class instance and any outputs or operations with the classes will need to take this into account. The implementation of the one dimensional Fourier transform is presented in figure 4.12.

The secondary set of functionality provided by the basis classes are mathematical operators on the functions the coefficients represent. There are four operators implemented, which are the addition, subtraction, derivative, and antiderivative operators. These four operations can be further categorized into arithmetic and calculus operations. The arithmetic operations, which are addition and subtraction, are implemented by following how the actual mathematical operations would be carried out on two functions which are Fourier series as shown in equation (4.23). For subtraction, the plus sign is simply replaced with the minues sign.

$$\sum_k \hat{u}_k e^{2\pi ikx} + \sum_k \hat{f}_k e^{2\pi ikx} = \sum_k \left(\hat{u}_k + \hat{f}_k\right) e^{2\pi ikx} \tag{4.23}$$

The implementation leverages the operator overloading in Python classes. For addition, the overload should be done to the `__add__` function. This function adds the current instance to another object which is the other basis instance for our use case. We also want the operation to return an independent instance without any references to the previous instances. To do this, all properties are coppied into a new instance. This is then used to perform the arithmetic operation. The implementation in figure 4.13 demonstrates the addition operation. For subtraction, a similar implementation is done using the `__sub__` function and switching the plus sign with the minus sign.

```
...
    def __add__(self, other: Self):
        if isinstance(other, self.__class__):
            if other.coeff is None:
                return self.copy()
            elif self.coeff is None:
                return other.copy()
            else:
                result = self.resize_modes(other)
                result.coeff = result.coeff + other.coeff
                return result
        else:
            raise TypeError(
                f"unsupported operand type(s) for +: '{
                    self.__class__
                }' and '{type(other)}'"
            )
...
```

Figure 4.13: Implementation of basis addition function.

The calculus operations for Fourier basis take advantage of the properties of the Fourier series. As discussed in section 2.1, derivatives and integration become multiplication and division in the spectral space of Fourier series. Our implementation takes advantage of this as shown in figure 4.14. Similar to how subtraction is just a modification of the addition operation, the integral or antiderivative operator is also implemented simply by changing the operation with the term multiplier from multiplication to division.

```
...
    def grad(self, dim: int = 0, ord: int = 1) -> Self:
        copy = self.copy()
        if dim == 0 and self.time_dependent:
            # time dependent use finite differences
            dt = self.periods[0] / (self.time_size - 1)
            coeff = copy.coeff
            for o in range(ord):
                coeff = torch.gradient(coeff, spacing=dt, dim=1)[0]
            copy.coeff = coeff
        else:
            if self.time_dependent:
                # disregard time dimension
                dim = dim - 1
            k = copy.wave_number(copy.modes[dim])
            multiplier_dims = [1 for _ in range(copy.ndim)]
            multiplier_dims[dim] = copy.modes[dim]
            if self.time_dependent:
                multiplier_dims = (1, *multiplier_dims)
            multiplier = (
                2
                * torch.pi
                * 1j
                * k.reshape(multiplier_dims).to(copy.coeff)
                / self.periods[dim]
            )
            multiplier = multiplier.pow(ord)
            coeff = copy.coeff.mul(multiplier)
            coeff[:, ..., 0] = torch.tensor(0 + 0j)
            copy.coeff = coeff
        return copy
...
```

Figure 4.14: Implementation of basis grad function.

The last group of functionality implemented in the Basis and FourierBasis classes provides convenience and often used procedures when working with basis functions. First, random coefficient generation for the Fourier basis is implemented. This is done as discussed in step 3 of the data generation process discussed in section 4.1. The implemented function shown in figure 4.15 is then wrapped in another function that creates a new FourierBasis instance with the generated coefficients.

```
...
    @classmethod
    def generate_coeff(
        cls,
        n: int,
        modes: int | tuple[int, ...],
        generator: torch.Generator | None = None,
        random_func: Callable[..., torch.Tensor] = torch.randn,
        complex_funcs: bool = False,
        scale: bool = True,
    ) -> torch.Tensor:
        if isinstance(modes, int):
            modes = (modes,)
        n_modes = len(modes)
        assert n_modes > 0, "modes should have at least one element"
        random_func = partial(random_func, generator=generator)
        if complex_funcs:
            coeff = random_func((n, *modes), dtype=torch.complex64)
        else:
            coeff = random_func((n, *modes), dtype=torch.complex64)

            vals = cls.inv_transform(coeff)
            coeff = cls.transform(vals.real + 0j)
        if scale:
            scaler = torch.tensor(modes).sum() * 0.2
            coeff = coeff.mul(scaler)
        return coeff
...
```

Figure 4.15: Implementation of Fourier Basis coefficient generation function.

Other convenience functionality also provided include plotting, function value perturbation, and function value evaluation based on domain span information that has been stored in the class instance. The function value evaluation is especially useful for experimenting and for the plotting functionality itself. This is because, the span was given to the constructor and does not need to be composed again with the inverse transform function.

Model

The SpectralSVR model is implemented in this module. There are two components in this module. First, there is the implementation of least-squares support vector regression (LSSVR) using Pytorch. This implementation is a reimplementation and modification of an LSSVR implementation using scikit-learn by Florêncio et al.

(2020). The modifications are mainly concerned with using Pytorch in place of scikit-learn. Other modifications are concerned with the performance side of things, which are computing the kernel matrix in batches to avoid memory spikes and the ability to compute on hardware accelerators supported by Pytorch such as GPUs. The LSSVR implementation starts with the constructor which accepts model hyperparameters which include the regularization parameter, kernel function and any kernel parameters, verbosity level, kernel matrix computation batch size, and device to perform computations on. The recieved parameters are then stored as properties of the class instance. For the kernel specifically, it will be initialized with the correct default parameters when the fitting function is called. This is because if the kernel of choice is the radial basis function, the default scaling parameter needs to be computed from the training features as the square root of the sum of feature variance values.

The optimization function that fits the model to the training data solves equation (2.10). This function is shown in figure 4.16. The first half of the function sets up the left and right hand side matrices. The left hand side matrix is constructed in part with the kernel matrix. The kernel function used is batched to reduce the peak memory footprint. These matrices are then used in the second half to compute the solution using the least squares solver function from Pytorch called lstq. Finally, the result is split into the biases and Lagrange multipliers which are then returned as a tuple. The optimizing function is wrapped in a more user-friendly function which allows the use of numpy arrays in addition to the Pytorch Tensor used in the optimizing function. The wrapper function is named fit. It conforms the inputs provided by the user into the expected types and matrix shapes of rows for samples and columns for input features or output targets. The processed inputs and outputs are also stored as support vectors for use during prediction. The fit function returns the class instance once training is done. This is for method chaining purposes for ease of use when using the fit function in a chain with other functions we will discuss next, such as the prediction function.

```
...
    def _optimize_parameters(
      self,
      X: torch.Tensor,
      y_values: torch.Tensor,
    ):

        A = torch.empty(
          (X.shape[0] + 1,) * 2,
          device=self.device,
          dtype=self.dtype,
        )
        A[1:, 1:] = self._batched_K(X, X)
        A[1:, 1:].diagonal().copy_(
            A[1:, 1:].diagonal()
            + torch.ones(
                (A[1:, 1:].shape[0],),
                device=self.device,
                dtype=self.dtype,
            ).to()
            / self.C
        )
        A[0, 0] = 0
        A[0, 1:] = 1
        A[1:, 0] = 1
        shape = np.array(y_values.shape)
        shape[0] += 1
        B = torch.empty(
          list(shape), device=self.device, dtype=self.dtype
        )
        B[0] = 0
        B[1:] = y_values

        solution: torch.Tensor = torch.linalg.lstsq(
            A.to(dtype=torch.float), B.to(dtype=torch.float)
        ).solution.to(dtype=self.dtype)

        b = solution[0, :]
        alpha = solution[1:, :]

        return (b, alpha)
...
```

Figure 4.16: Implementation of Least-squares Support Vector Regression fitting function.

The learned multipliers and bias parameters are then used for predicting outputs from unseen sample features. Equation (4.20) shows the computation that needs to

be done to compute the predicted output. The prediction process first constructs both matrices on the left-hand side of the equation. This is done by computing the kernel matrix between the prediction features and the training features, otherwise known as support vectors. The prediction function therefore is very straight forward with an input of unseen features and the learned parameters. The function output is simply the predicted outputs. The implementation of this function is shown in figure 4.17.

```
...
NumpyArrayorTensor = (
    np.ndarray[typing.Any, np.dtype[np.float_]] |
    torch.Tensor
)
...
    def predict(
        self,
        X: NumpyArrayorTensor,
    ) -> NumpyArrayorTensor:
        """Predicts the labels of data X given a trained model.
        - X: ndarray of shape (n_samples, n_attributes)
        """
        is_torch = isinstance(X, torch.Tensor)
        if is_torch:
            if X.ndim == 1:
                X_reshaped_torch = X.reshape(-1, 1)
            else:
                X_reshaped_torch = X
            X_= X_reshaped_torch.clone().to(
                self.device, dtype=self.dtype
            )
        else:
            if X.ndim == 1:
                X_reshaped_np = X.reshape(-1, 1)
            else:
                X_reshaped_np = X
            X_ = torch.from_numpy(X_reshaped_np).to(
                self.device, dtype=self.dtype
            )

        KxX = self._batched_K(X_, self.sv_x)

        y_pred = KxX @ self.alpha + self.b
        predictions: NumpyArrayorTensor
        if is_torch:
            predictions = y_pred.to(X)
        else:
            predictions = y_pred.cpu().numpy()

        if X.ndim == 1:
            return predictions.reshape(-1)
        else:
            return predictions
...
```

Figure 4.17: Implementation of Least-squares Support Vector Regression prediction function.

Aside from these core functions, interpretation of the model using the methods introduced by Üstün et al. (2007) are also implemented in the LSSVR class. First, using the support vectors and the kernel matrix computed between each support vectors, the correlation image is computed. This image, which is a correlation matrix, is intended to visualize the importance of features within kernel functions. This is simply computed with matrix multiplication between the kernel matrix and the support vectors. The implementation is shown in figure 4.18. The batched kernel function is used in this case to mitigate the memory footprint.

```
...
    def get_correlation_image(self):
        return self._batched_K(
            self.sv_x, self.sv_x
        ).mm(self.sv_x)
...
```

Figure 4.18: Implementation of Least-squares Support Vector Regression correlation image function.

The other interpretation method introduced by Üstün et al. (2007) visualizes the relationship learned between the input features and the outputs. This visualization is computed as the matrix multiplication between the support vectors and the learned Lagrange multipliers. The support vector matrix is transposed so that the multiplication is done on the dimension that indexes each sample. This computation is implemented as shown in figure 4.19. The resulting matrix is termed the p-matrix. The columns of this matrix represents the outputs and the rows represents the input features. The p-matrix values show how each feature contribute to the output learned by the model.

```
...
    def get_p_matrix(self):
        return self.sv_x.T.mm(self.alpha)
...
```

Figure 4.19: Implementation of Least-squares Support Vector Regression p-matrix function.

The second component of the model modules is the SpectralSVR implementation that uses a multi-output support vector regression (SVR) model to learn in the spectral

domain, such as the LSSVR implementation in the first component. The SpectralSVR is implemented as a class that extends the LSSVR to be able to learn from features and labels which are complex valued, which is the case for Fourier series coefficients. First, the constructor used to initialize each SpectralSVR instance accepts a Basis instance, an SVR instance which is the implemented LSSVR by default, and the verbosity of the model. These parameters are then used when the training function shown in figure 4.20 is called. Training the SpectralSVR model begins by calling the train function with parameters of the input function representation, output function representation, and an indicator of whether the output function is time dependent. Then, the function ensures that the features and labels are matrices. And then, if the input or output function representations are complex, they are transformed into the real representation. These formatted training data features and labels are then used to train the LSSVR model itself. Finally, to again allow for chaining methods, the function returns the current class instance.

```
...
    def train(
        self,
        f: torch.Tensor,
        u_coeff: torch.Tensor,
        u_time_dependent: bool = False,
    ):
        self.basis.time_dependent = u_time_dependent
        if self.basis.coeff_dtype.is_complex:
            u_coeff = to_complex_coeff(u_coeff)

        if f.ndim > 2:
            f = f.flatten(1)
        if u_coeff.ndim > 2:
            u_coeff = u_coeff.flatten(1)

        if torch.is_complex(u_coeff):
            u_coeff = to_real_coeff(u_coeff)
        if torch.is_complex(f):
            f = to_real_coeff(f)
        self.svr.fit(f, u_coeff)
        return self
...
```

Figure 4.20: Implementation of SpectralSVR training function.

Using the learned data to predict other output function representations from unseen

input functions can be done by directly calling the predict function of the LSSVR. This results in the real representation which needs to be converted into the complex representation for the FourierBasis. Once the conversion is done, the coefficients can be used to construct a new FourerBasis instance of the predictions. From there, the predicted functions can be evaluated and plotted. However, if one simply wants to evaluate the value of the predicted function at arbitrary points, another function is implemented to provide ease of use for this exact case. The implemented function is called forward as displayed in figure 4.21. The arguments to this function are the input functions, the evaluation points, and the domain span. The function first predicts the output function coefficients. Then, the predicted coefficients are multiplied with the basis function values at each point to compute the final predicted point values.

```
...
    def forward(
        self,
        f: torch.Tensor,
        x: torch.Tensor,
        periods: tuple[float, ...]
        | None = None,
    ) -> torch.Tensor:
        if len(x.shape) == 1:
            x = x.unsqueeze(-1)

        # compute coefficients
        if torch.is_complex(f):
            f = to_real_coeff(f)
        coeff = self.svr.predict(f)
        # convert to complex if basis needs complex values so that the reshaping
        if self.basis.coeff_dtype.is_complex:
            coeff = to_complex_coeff(coeff)

        return self.basis.evaluate(
            coeff=coeff.reshape((f.shape[0], *self.modes)),
            x=x,
            periods=periods,
            time_dependent=self.basis.time_dependent,
        )
...
```

Figure 4.21: Implementation of SpectralSVR forward function (pointwise prediction).

The final core piece of functionality the SpectralSVR class provides is the inverse parameter estimation. This is implemented to solve inverse problems such as predicting

the initial conditions for the Burgers' equation or heat equation. This function essentially does the gradient descent on a loss function in such a way that the output function matches some expected output. The loss function is simply a measure of how far the outputs of the current predicted inputs are from the target outputs. The loss function is formulated as the mean squared error of the difference between the predicted output and expected output. Using some randomly initialized values as the inputs, the predicted output is then used to compute the loss. The gradient of the loss with respect to the inputs are then computed and then used to perform optimization of the inputs using the ADAM optimizer. This is implemented as the inverse function shown in figure 4.22. The function arguments are the expected output function coefficients, evaluation points, the loss function used, how many optimization loops are done, the random number generator, and the gain which is used in generating the random initial input functions. The function returns the estimated input function coefficients in the real representation. For Fourier coefficients this means that the predicted input coefficients need to first be converted to complex valued tensors and then used to construct a FourierBasis instance. For convenience, a wrapper like the forward function is also implemented for evaluating the function values of the predicted input coefficients.

```
...
    def inverse_coeff(
        self,
        u_coeff: torch.Tensor,
        loss_fn: Callable[
            [torch.Tensor, torch.Tensor], torch.Tensor
        ] = mean_squared_error,
        epochs=100,
        generator=torch.Generator().manual_seed(42),
        gain=0.05,
        **optimizer_params,
    ):
        f_shape = (u_coeff.shape[0], self.svr.sv_x.shape[1])
        complex_coeff = u_coeff.is_complex()
        original_device = u_coeff.device
        u_coeff = to_real_coeff(u_coeff.flatten(1)).to(self.svr.device)

        # inverse problem
        f_coeff_pred = (
            torch.randn(f_shape, generator=generator).to(self.svr.device) * gain
        )
        f_coeff_pred.requires_grad_()
        optim = torch.optim.Adam([f_coeff_pred], **optimizer_params)

        for epoch in range(epochs):
            optim.zero_grad()
            u_coeff_pred = self.svr.predict(f_coeff_pred)
            loss = loss_fn(u_coeff_pred, u_coeff)
            loss.backward()
            optim.step()
        optim.zero_grad()
        f_coeff_pred.requires_grad_(False)
        if complex_coeff:
            f_coeff_pred = to_complex_coeff(f_coeff_pred)
        return f_coeff_pred.to(original_device)
...
```

Figure 4.22: Implementation of SpectralSVR inverse coeff function (parameter estimation).

The SpectralSVR class also provides a convenience function for testing the performance of the learned model. This function is shown in figure 4.23. The function arguments are the testing inputs, expected testing outputs, and a resolution for evaluation of function values. The first step is to convert the testing input into real representations and then predicting the output function. The predicted output are then compared to the testing outputs using many metrics including RMSE, MSE, MAE, R2,

SMAPE, RSE, RRSE, and the number of Nan values present in the predicted output. The same comparison process is carried out again for the function values which are evaluated at the specified resolution. Finally, the function returns the metric values as a nested tuple for both the coefficients predictions and the function value predictions.

```
...
    def test(
        self,
        f: torch.Tensor,
        u_coeff_targets: torch.Tensor,
        res: ResType = 200,
    ):
        if torch.is_complex(f):
            logger.debug("transform f to real")
            f = to_real_coeff(f)
        u_coeff_preds = self.svr.predict(f)
        if torch.is_complex(u_coeff_targets):
            logger.debug("transform u_coeff to real")
            u_coeff_targets = to_real_coeff(u_coeff_targets)

        grid = self.basis.grid(res).flatten(0, -2)
        u_preds = self.basis.evaluate(
            coeff=to_complex_coeff(u_coeff_preds),
            x=grid,
            time_dependent=self.basis.time_dependent,
        ).real
        u_targets = self.basis.evaluate(
            coeff=to_complex_coeff(u_coeff_targets),
            x=grid,
            time_dependent=self.basis.time_dependent,
        ).real
        return {
            "spectral": get_metrics(
                u_coeff_preds, u_coeff_targets
            ),
            "function value": get_metrics(u_preds, u_targets),
        }
...
```

Figure 4.23: Implementation of SpectralSVR test function.

Problems

The final module implements the PDEs that will serve as problems the proposed modules will solve. The implementation is mainly responsible for generating datasets from the PDEs and computing the PDE residuals. This implementation is focused

on the two synthetic datasets which are the antiderivative problem and the Burgers' equation problem. The problem base class is implemented as an abstract class that the specific problems will subclass. The base class requires any subclass to implement three methods. First, the data generation method which receives specifications such as what basis functions to use, how many function samples to create, how many modes are needed for each sample, and a Pytorch generator that will be used in generating the random basis coefficients. Other arguments more specific to each problem will be implemented by the specific subclass. This function is then expected to return a tuple of Basis instances. The second and third functions are the spectral and function value residuals for the PDE of each subclass, respectively. These three functions make up the functionality that is offered by all Problem subclasses. The implementation of the Problem subclass can be seen in figure 4.24.

```python
import abc
import torch
from ..basis import BasisSubType

class Problem(abc.ABC):
    def __init__(self) -> None:
        super().__init__()

    @abc.abstractmethod
    def generate(
        self,
        basis: type[BasisSubType],
        n: int,
        modes: int | tuple[int, ...],
        *args,
        generator: torch.Generator | None = None,
        **kwargs,
    ) -> tuple[BasisSubType, ...]:
        pass

    @abc.abstractmethod
    def spectral_residual(
        self, u: BasisSubType, *args, **kwargs
    ) -> BasisSubType:
        pass

    @abc.abstractmethod
    def residual(
        self, u: BasisSubType, *args, **kwargs
    ) -> BasisSubType:
        pass
```

Figure 4.24: Implementation of Problem base class.

The antiderivative problem is relatively simple to implement. The generation function takes advantage of the gradient operation and generate function provided by the Basis subclasses. The arguments to this function are the same as the base class with the addition of an integration constant parameter. By default, the value of the integration constant is zero. The function then returns the tuple of basis subclass instances representing the derivative and antiderivative functions. This function can be seen in figure 4.25.

```
...
    def generate(
        self,
        basis: Type[BasisSubType],
        n: int,
        modes: int | tuple[int, ...],
        u0: float | int | complex,
        *args,
        generator: torch.Generator | None = None,
        **kwargs,
    ) -> tuple[BasisSubType, BasisSubType]:
        if isinstance(modes, int):
            modes = (modes,)
        # generate solution functions
        u = basis.generate(
            n, modes, generator=generator, *args, **kwargs
        )
        # compute derivative functions
        ut = u.grad()
        # set the integration coefficient
        if isinstance(u0, complex):
            if u.coeff.is_complex():
                u.coeff[:, 0] = torch.tensor(u0)
            else:
                u.coeff[:, 0] = torch.tensor(u0).real
        elif isinstance(u0, float) or isinstance(u0, int):
            if u.coeff.is_complex():
                u.coeff[:, 0] = torch.tensor(u0 + 0j)
            else:
                u.coeff[:, 0] = torch.tensor(u0)
        else:
            u.coeff[:, 0] = u0

        return (u, ut)
...
```

Figure 4.25: Implementation of Antiderivative generate function.

The residual functions are similarly easy to implement as shown in figure 4.26.

```
...
    def spectral_residual(
        self, u: BasisSubType, ut: BasisSubType
    ) -> BasisSubType:
        residual = u.grad() - ut
        if residual.coeff is not None:
            residual.coeff[:, 0].mul_(0)

        return residual

    def residual(
        self, u: BasisSubType, ut: BasisSubType
    ) -> BasisSubType:
        u_val, grid = u.get_values_and_grid()
        ut_val = ut.get_values()
        dt = grid[1, 0] - grid[0, 0]
        u_grad = torch.gradient(
            u_val, spacing=dt.item(), dim=1
        )[0]
        residual_val = u_grad - ut_val
        residual = u.copy()
        residual.coeff = u.transform(residual_val)
        return residual
...
```

Figure 4.26: Implementation of Antiderivative residual functions.

For the Burgers' equation, the problem subclass for this PDE implemented a generate function with two generation paths. But before discussing the specifics of the two paths, the function has some extra arguments and preprocessing of those arguments. This time the function asks for the kind of functions the initial condition and the forcing term needs to be, whether they are random or constant. The combination of the kind of functions the initial conditions and forcing terms are will determine the path of generation that the function will take. The function also requires the viscosity parameter nu which is 0.01 by default. The domain also needs to be specified with a default value of 0 to 1 with 200 grid points for both space and time. The solver which is used for one of the generation procedures is also an argument with a default of the implicit adams solver from torchdiffeq (R. T. Q. Chen, 2021). Finally, whether the output basis coefficients are time dependent or not is passed in as an argument alongside with the Pytorch generator. The implementation of this portion of the function can be seen in figure 4.27.

```
...
    def generate(
        self,
        basis: Type[BasisSubType],
        n: int,
        modes: int | tuple[int, ...],
        u0: ParamInput | BasisSubType = "random",
        f: ParamInput | BasisSubType = 0,
        nu: float = 0.01,
        space_domain=slice(0, 1, 200),
        time_domain=slice(0, 1, 200),
        solver: SolverSignatureType = implicit_adams_solver,
        time_dependent_coeff: bool = True,
        *args,
        generator: torch.Generator | None = None,
        **kwargs,
    ) -> tuple[BasisSubType, BasisSubType]:
        if isinstance(modes, int):
            modes = (modes,)

        device = "cuda:0" if torch.cuda.is_available() else "cpu"

        L = space_domain.stop - space_domain.start
        x = (
            basis.grid(slice(
                space_domain.start, space_domain.stop, modes[0]
            )).flatten(0, -2)
            .to(device=device)
        )
        T: float = time_domain.stop - time_domain.start
        nt = int(time_domain.step)
        # nt = int(T / (0.01 * nu) + 2)
        dt = T / (nt - 1)
        t = basis.grid(time_domain).flatten().to(device=device)
        periods = (T, L)
...
```

Figure 4.27: Implementation of Burgers generate function.

The first generation path and most similar to the antiderivative case is when both the initial condition and forcing terms are random. This branch of the generate function utilizes the residual function to compute the forcing term from the randomly generated solution function. This method of generating the solution and forcing term is stable and relatively straightforward. The implementation of this branch is shown in figure 4.28.

```
...
        if u0 == "random" and f == "random":
            # use method of manufactured solution
            time_mode = modes[0]
            if len(modes) > 1:
                modes = modes[1:]
            u = basis.generate(
                n,
                (time_mode, *modes),
                periods=periods,
                generator=generator,
            )
            res_modes = tuple(slice(0, L, mode) for mode in modes)
            fst = self.spectral_residual(
                u,
                basis(
                    basis.generate_empty(n, (time_mode, *modes))
                ),
                nu,
            )
            u_gen = u
            f_gen = fst
            # convert to timed dependent coeffs
            if time_dependent_coeff:
                u_val = u.get_values(res=(time_domain, *res_modes))
                u_coeff = basis.transform(
                    u_val.flatten(0, 1)
                ).reshape((n, nt, *modes))
                u_gen = basis(
                    coeff=u_coeff,
                    time_dependent=True,
                    periods=periods
                )

                f_val = fst.get_values(
                    res=(time_domain, *res_modes)
                )
                f_coeff = basis.transform(
                    f_val.flatten(0, 1)
                ).reshape((n, nt, *modes))
                f_gen = basis(
                    coeff=f_coeff,
                    time_dependent=True,
                    periods=periods
                )
...
```

Figure 4.28: Implementation of Burgers generate function manufactured method.

The second case is when at least one of the initial condition or forcing term is not random. This second case requires solving the Burgers' equation using traditional numerical methods. The generate function calls a function that has the responsibility of setting up the constant initial conditions or constant forcing terms and then calls the ODE solver specified in the generate function arguments. The right-hand side function computes the time derivative based on equation (4.17). The implementation of this is show in figure 4.29. Putting the above together gives us the implementation of the method of lines generation of Burgers' equation solution and forcing term as show in figure 4.30.

```
...
    @staticmethod
    def rhs(
        basis: type[Basis],
        nu: float,
        u_hat: torch.Tensor,
        f_hat: torch.Tensor,
    ) -> torch.Tensor:
        u = basis(u_hat)
        dealias_modes = tuple(
            int(mode * 1.5) for mode in u.modes
        )
        u_dealiased = u.resize_modes(
            dealias_modes, rescale=False
        )
        u_val = basis.inv_transform(u_dealiased.coeff)
        uu_x_hat_dealiased = 0.5 * basis.transform(u_val**2)
        uu_x = basis(
            uu_x_hat_dealiased
        ).resize_modes(u.modes, rescale=False).grad()

        u_u_x_hat = uu_x.coeff
        u_xx_hat = u.grad().grad().coeff
        u_t_hat = nu * u_xx_hat + f_hat - u_u_x_hat
        return u_t_hat
...
```

Figure 4.29: Implementation of Burgers generate function time derivative.

```
...
        u0.coeff = u0.coeff.to(device=device)
        fst.coeff = fst.coeff.to(device=device)
        print(f"generating with {len(t)} time steps")

        def f_func(t: torch.Tensor, x: torch.Tensor = x):
            x = x.tile((1, 2))
            x[:, 0] = t
            return basis.transform(
                fst(x).reshape((-1, modes[0]))
            )

        def rhs_func(t: torch.Tensor, y0: torch.Tensor):
            y0 = to_complex_coeff(y0)
            return to_real_coeff(
                cls.rhs(basis, nu, y0, f_func(t))
            )

        u_hat = solver(rhs_func, to_real_coeff(u0.coeff), t)
        if basis.coeff_dtype.is_complex:
            u_shape = u_hat.shape
            u_hat = to_complex_coeff(
                u_hat.flatten(0, 1)
            ).reshape(
                (*u_shape[:2], *u0.coeff.shape[1:])
            )

        u_hat = u_hat.movedim(0, 1)
        if timedependent_solution:
            u = basis(u_hat, **kwargs, time_dependent=True)
        else:
            u_hat = u_hat.reshape((n * nt, modes[0]))
            u = basis(
                basis.transform(
                    basis.inv_transform(u_hat).reshape(
                        (n, nt, modes[0])
                    )
                ),
                **kwargs,
            )
        u.coeff = u.coeff.cpu()
        fst.coeff = fst.coeff.cpu()
        return (u, fst)
...
```

Figure 4.30: Implementation of Burgers generate function method of lines.

The spectral residual of the Burgers' equation which is used in the method of

manufactured solution generation approach is implemented as shown in figure 4.31. As with the right hand side function, we use the psuedospectral approach for computing the convolution term to avoid large computational expenses for higher number of modes. The function value residual is also implemented in a similar manner to the antiderivative version. The derivatives are computed with the Pytorch gradient function. And then using equation (4.7), the residual is computed by subtracting the forcing term from both sides.

```
...
    def spectral_residual(
        self, u: BasisSubType, f: BasisSubType, nu: float
    ) -> BasisSubType:
        u_t = u.grad(dim=0, ord=1)

        dealias_modes = tuple(
            int(mode * 1.5) for mode in u.modes
        )
        u_dealiased = u.resize_modes(
            dealias_modes, rescale=False
        )
        u_val = u.inv_transform(u_dealiased.coeff)
        uu_dealiased = u.copy()
        uu_dealiased.coeff = u.transform(u_val.pow(2).mul(0.5))
        uu_x = uu_dealiased.resize_modes(
            u.modes, rescale=False
        ).grad(dim=1)

        u_xx = u.grad(dim=1, ord=2)
        nu_u_xx = u_xx
        nu_u_xx.coeff = nu_u_xx.coeff * nu

        residual = u_t + uu_x - nu_u_xx - f
        return residual
...
```

Figure 4.31: Implementation of Burgers spectral residual function.

4.4.4 Testing

The implementation is followed by tests of the functionality core to this study. The testing is done using the pytest library. The testing method used is a black box approach. The tests are written in a separate `tests` directory. Each module is tested by a separate file. The tests are done to ensure compliance of the implementation to the requirements of the software. The final results are presented in table 4.1. Each version and iteration of

the development must ensure that the tests are passed before any changes are committed to the Github repository.

No	Process	Test Target	Test Result
1	Transform	Transform invertible with inverse transform	Achieved
2	Evaluation	Transform coefficient evaluation close to original values	Achieved
3	Plot	Plotting function is run successfully	Achieved
4	Perturb	Perturb function is run successfully	Achieved
5	Operations	Operation functions is run successfully	Achieved
6	Complex Coefficients Conversion	Conversion between real and complex coefficient representation is invertible for odd and even number of modes	Achieved
7	SpectralSVR Train	Training function is run successfully	Achieved
8	SpectralSVR Prediction	Coefficient prediction error within tolerable range	Achieved
9	SpectralSVR Prediction	Function value prediction error within tolerable range	Achieved

Table 4.1: Testing results of the SpectralSVR Library implementation using black box method.

4.5 Experimental Scenarios

To achieve the goals of this study, as outlined in section 1.3, we lay out three experimental scenarios. These scenarios represent different experimental configurations that will be applied to our implementation of the SpectralSVR library. A table of the configurations for each scenario can be seen in table 4.2.

Table 4.2: The configuration of experimental scenarios in this study.

Configuration	Scenario 1	Scenario 2	Scenario 3
Data Source	Synthetic (computed from equations)	Synthetic (computed from equations) with three viscosity values	ERA5 dataset
Data Augmentations	Perturbations of three different noise levels	Perturbation of 10% the mean standard deviation of function values	
Data Sample Size	5000 unique functions for each noise level	500 unique functions for each viscosity value	7000 time steps
Number of Modes			
Scaling	Standard scaling	Standard scaling	Standard scaling
Dataset Split	80% Training and 20% Testing for each noise level	80% Training and 20% Testing for each viscosity value	80% Training and 20% Testing
Regularization Parameter (C)	1.0	1.0	1.0
Kernel	RBF ($\sigma = features \times X.var()$)	RBF ($\sigma = features \times X.var()$)	RBF ($\sigma = features \times X.var()$)
Additional Tests	Exact solutions	Exact solutions	
Interpretation	p-matrix and correlation image	p-matrix and correlation image	p-matrix and correlation image

Each scenario serves a different purpose. The first scenario is constructed to establish whether the model can learn any relationships at all in data that implicitly defines differential equations. This scenario is a proof of concept of whether the model is capable of accurately learning the relationship between derivatives and their anti-derivatives. As the simplest case, it provides a foundation for understanding the model and its behavior. The 5% noise model is then used to predict the antiderivative

of a cosine function with a period of one as shown in equation (4.24). The exact solution is known as equation (4.25) (Abramowitz & Stegun, 1972). The second goal of this scenario is to determine how noise affects the model's predictions. This is especially important for the inverse problem because of how sensitive the derivative is to changes in the antiderivative. To further solidify how the model fares for inverse problems, this scenario will also assess the performance of a trained model for a very simple inverse problem setup to determine the derivatives of the testing subset from the antiderivatives. This setup will utilize the model as a surrogate forward solver and optimize for a loss function using the inverse function of the SpectralSVR class as described in section 4.4.3.

$$f(x) = 2\pi cos\,(2\pi x) \tag{4.24}$$

$$f(x) = sin\,(2\pi x) \tag{4.25}$$

The second scenario extends the goal of the first scenario by examining the model and its behavior when learning a nonlinear PDE. The data subsets with different viscosity values are intended to allow us to learn more about how this will affect the performance on the exact solutions which may contain discontinuities for lower viscosity numbers. The model will learn to predict future states of systems governed by the Burgers' equation from past states. The model trained for a viscosity value of 0.01 will be used to predict equation (4.8) from initial conditions at time equals zero and the corresponding forcing term of a constant value of zero.

The third scenario is designed to demonstrate the modeling capability of SpectralSVR on a more practical problem of weather prediction. The earth weather system is a complex collection of processes. Using the ERA5 dataset, the model will be used to predict future states of the atmosphere from previous states. Specifically, the model will learn to predict the temperature 2 meters above the surface. That means that other than the time and spatial resolution not being the highest, the model will also learn from partial information of the relationships defined by the equation since no other variables will be included. This choice was made as an analog for situation with unknown PDEs and therefore unknown variables. With these situations, there is no guarantee that the variables measured have any relation with the system. These three scenarios together address the last two aims of this study.

4.6 Experimental Results

In this section, the results of each experimental scenario is presented and analyzed. The results come in the form of testing metrics mentioned in . The model interpretations are displays of the correlation image and the p-matrix. The function values and coefficients themselves will also be plotted depending on the number of dimensions.

4.6.1 Scenario 1

The first scenario results are presented in four parts. The first is the coefficient prediction metrics which is shown in table 4.3. The table shows the noise level, the corresponding kernel scaling factor sigma, and the performance metrics themselves.

Table 4.3: Performance metrics of coefficient prediction in scenario 1 by noise level.

Noise level	Sigma	MSE	RMSE	MAE	R2	sMAPE
5%	10.00	0.85	0.92	0.56	0.96	0.31
10%	10.00	2.07	1.44	0.93	0.91	0.46
50%	10.00	15.56	3.94	3.04	0.50	1.04

The scenario is implemented as a Jupyter notebook which imports relevant libraries and our SpectralSVR library. The notebook starts with creating the data with the Antiderivative problem subclass. All random processes use the same Pytorch Generator instance with a seed of 42. The data is then augmented by perturbing the function values to create three versions with the noise levels mentioned in the scenario. Looping through each version, the training and testing subsets are randomly sampled to result in 80% and 20% of the original dataset respectively. Then the scaler is fitted on the training subset inputs. And then, both the training and testing inputs are transformed using the fitted scaler. Next, an instance of SpectralSVR is trained and tested. Finally, the metrics are stored and the next noise level is processed. Next the 5% noise model is used to predict the antiderivative of a sine function.

Table 4.3 shows that the model is able to generalize from the training data and learn the simple linear antiderivative operator. Focusing on the coefficient of determination (R2) scores, we can see that the model is off by 0.04 to the perfect score of 1.0 for the lowest noise level. While increasing noise levels does degrade the performance,

this is partly due to the target values also having been perturbed. This fact can be seen if we look at how predictions from the very same trained models on noisy inputs are compared to the noise-free versions of the antiderivative functions which is shown in table 4.4. The metrics show that the model predictions are slightly closer to the unperturbed function coefficients compared to the perturbed versions. This can be seen as the influence of the independent synthetic measurement noise in the perturbed targets being removed from the testing metrics.

The higher noise levels shows that the model is still relatively accurate. Looking at the R2 score for the 50% noise level, the model is more accurate than a baseline mean value model. The R2 score of 0.5 means that the model predictions has roughly half the error the baseline would produce. Another observation is that the kernel scaling hyperparameter sigma has the same value the same for all noise levels since the inputs are all scaled to approximately have a standard deviation of one. The value itself is from the number of features which comes out to 100 total inputs to the LSSVR.

Table 4.4: Performance metrics of coefficient prediction compared to unperturbed targets in scenario 1 by noise level.

Noise level	MSE	RMSE	MAE	R2	sMAPE
5%	0.78	0.89	0.51	0.96	0.28
10%	1.82	1.35	0.81	0.92	0.41
50%	9.34	3.06	2.25	0.62	0.91

The function values are also evaluated and the values of the metrics between the noisy targets and predictions are shown in table 4.5. While the relative metrics R2 and sMAPE stay close to the values we obtained for the coefficients themselves, since the metrics are now being computed in the physical domain, the scales have changed and because of that the values of the absolute metrics now reflect the change in scale. For reference, the scale of the target coefficient values for the 50% noise level dataset in their real representation can range on average from -13.54 to 13.6 across the entire dataset. Therefore, an RMSE value of 3.94 for the predictions compared to the noisy targets mean that the error ratio is roughly 0.148 or just above 1 to 7. For the function values of the 50% noise dataset the values range on average from -2.5 to 2.49. This was more difficult to compute since there is no direct way to compute the amplitude of the function from just the coefficients. Here we used the inverse transform and extracted

the maximum and minimum values of each function from the discrete values. Since the RMSE in table 4.5 for the 50% noise dataset is 0.63, the error ratio comes to 0.126. One side note about table 4.5 is that since the model instances are the same as the ones used in the coefficient evaluations, the hyperparameters are still the same including the kernel scaling factor sigma.

Table 4.5: Performance metrics of function value from evaluated coefficient prediction in scenario 1 by noise level.

Noise level	MSE	RMSE	MAE	R2	sMAPE
5%	0.03	0.18	0.15	0.97	0.39
10%	0.08	0.29	0.23	0.92	0.55
50%	0.62	0.79	0.63	0.49	1.04

For the metrics between the predictions and the noise-free version of the target function values, the results parallel the outcomes of the coefficient predictions. The metrics show that the model performs slightly better with more pronounced differences for the higher noise levels. This echoes our previous statement on the effect of independent "measurement" noise in the target values on the evaluation metrics.

Table 4.6: Performance metrics of function value from evaluated coefficient prediction compared to unperturbed targets in scenario 1 by noise level.

Noise level	MSE	RMSE	MAE	R2	sMAPE
5%	0.03	0.18	0.14	0.97	0.38
10%	0.07	0.27	0.22	0.92	0.53
50%	0.37	0.61	0.49	0.62	0.94

The next part of this scenario is the results from predicting the exact solution of equation (4.24) which is equation (4.25). The function values will be computed with the same discretization as the number of modes we used in the training set. Once the values are obtained for both functions, the coefficients are computed. Then instancing the FourierBasis class with the coefficients of the derivative function, we can create perturbed versions according to the noise levels of the training set. Finally, the derivative is used to predict the noise-free antiderivative. The results are presented in tables 4.7 and 4.8. For 5% and 10% noise levels, the model shows that it has learned

the relation. However, the 50% noise level, the model has been unable to predict the results well enough. The marked difference in error across all metrics between the 50% and the lower noise levels is more apparent for this specific exact problem compared to the test sets. A clear picture of this can be seen when we compare the sMAPE metric. For the test set, the predictions on average results in a value of 1, however, for this exact problem the sMAPE value is 1.4 to 1.7.

Table 4.7: Performance metrics of coefficient prediction of exact antiderivative in scenario 1 by noise level.

Noise level	MSE	RMSE	MAE	sMAPE
5%	0.12	0.35	0.20	1.26
10%	0.75	0.87	0.30	1.26
50%	10.35	3.22	0.82	1.39

Table 4.8: Performance metrics of evaluated function values of coefficient prediction of exact antiderivative in scenario 1 by noise level.

Noise level	MSE	RMSE	MAE	sMAPE
5%	0.01	0.07	0.06	0.24
10%	0.03	0.17	0.15	0.37
50%	0.41	0.64	0.57	1.66

The predictions of the exact equation is shown in figure 4.32. Visually, we can see that as the noise level increases, the model predictions become worse. Another observation is how the higher the noise level, the more the predicted functions become closer to zero. This is explained by the double penalty phenomenon (**lledoScaledependentVerificationPrecipitation2023**). The loss function used for LSSVR penalizes the model for predicting a non-zero value that turns out to be wrong compared to predicting a zero value. This results in a model with predictions that are close to the mean of the training data.

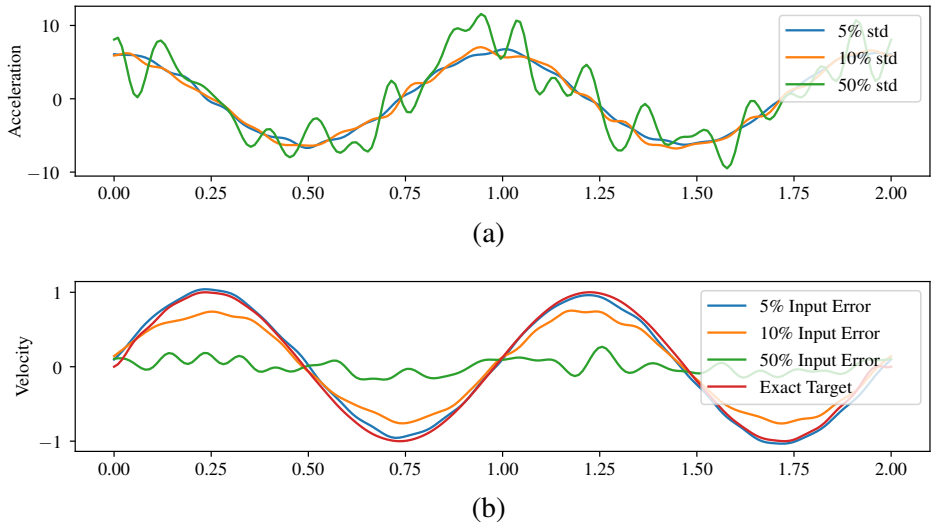

Figure 4.32: (a) The perturbed exact input function values from equation (4.24). (b) Prediction of antiderivative from the input function that was perturbed.

For inverse problems, we simply use the same testing set with the labels now used to predict the features. The model instances are still the same as before. With the implementation shown in figure 4.22, we run the inverse function for predicting coefficients with 2000 epochs, a learning rate of 0.02, and randomized starting point from a normal distribution multiplied by a factor of 0.05. The results of inverse prediction for all three noise levels are shown in table 4.9. These metrics were computed after both the target and predicted input functions are scaled back using the same scalers they were scaled down with. Because the scales of the input and output functions are different, the absolute metrics are much larger in these results compared to the forward problem results. For reference, the target input coefficents on average range from -695.65 to 694.9. The relative metrics show that for the lower noise levels, the accuracy is still relatively good. However, the values are lower than the values for the forward test. The difference with the antiderivative prediction becomes more pronounced with the higher noise levels. For the highest noise level, the performance has degraded so far that the predictions are worse than a baseline model from the mean of the target input functions. One must also note that despite the much worse results of the other metrics for the highest noise level, at this time we're unable to explain why sMAPE results in roughly the same performance as in the forward problem.

Table 4.9: Performance metrics of coefficient inverse prediction of derivative in scenario 1 by noise level.

Noise level	MSE	RMSE	MAE	R2	sMAPE
5%	1739.56	41.71	26.44	0.91	0.36
10%	3485.10	59.03	42.19	0.76	0.52
50%	49319.73	222.08	174.48	-0.19	1.05

Next, we have the correlation image and p-matrix for the model of each noise level. The results are shown in figure 4.33. Each row in the figure represent the results of a model trained on a different noise level. The correlation image for 5% and 10% noise show clear lines on the coefficient corresponding to the output coefficient that was sorted. We can also see that the negative wave number reflection also being sorted. This is because of the reflection that occurs with complex Fourier coefficients for real-valued functions. There are other faint vertical lines you are able to see for other input coefficients. These faint lines are not sorted like the corresponding coefficients we mentioned before. Meaning, while they don't affect the particular output coefficients that were sorted, they do show that there is information embedded in the kernel matrix for these input coefficients. However, if we look at the 50% noise correlation image, even the corresponding coefficient does not show a clear line or gradient. The lines are more noisy compared to the other noise levels. But the kernel still manages to embed some information. The p-matrices show that The model itself is able to still learn some relationship between the input coefficients and the output coefficients. For the 5% and 10% noise levels, the p-matrices show very clearly the contributions of input coefficients to the output coefficients. However, looking at the p-matrix for 50% noise level, the lower wave numbers show lower contribution of input coefficients to the output coefficients.

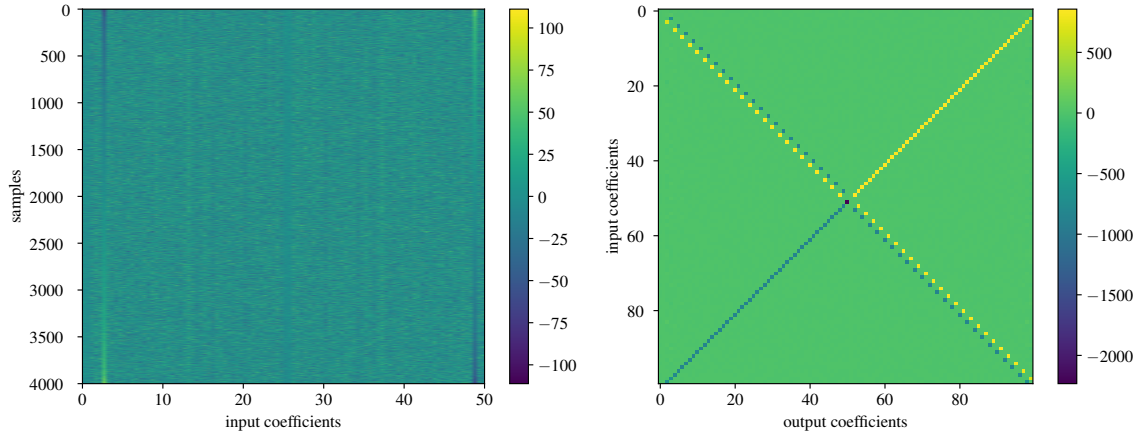

(a) Correlation image 5% noise.

(b) The p-matrix for 5% noise.

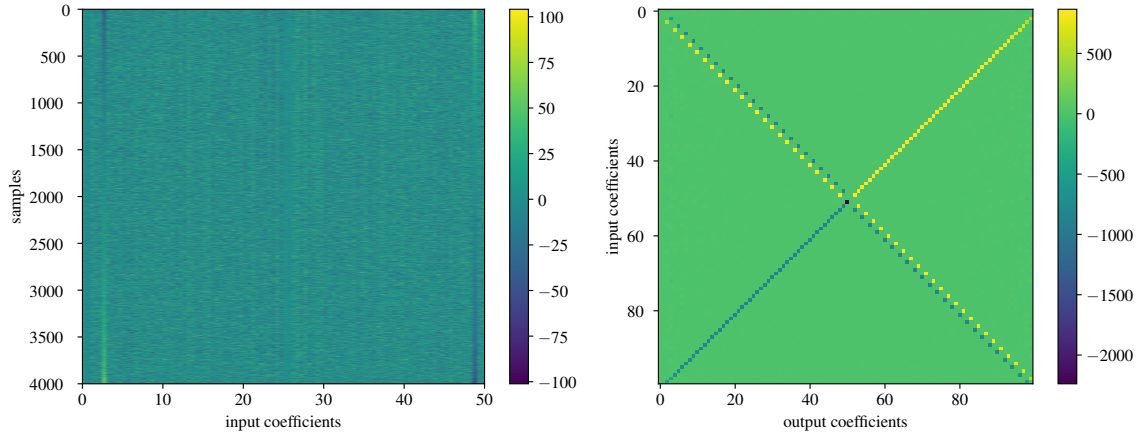

(c) Correlation image 10% noise.

(d) The p-matrix for 10% noise.

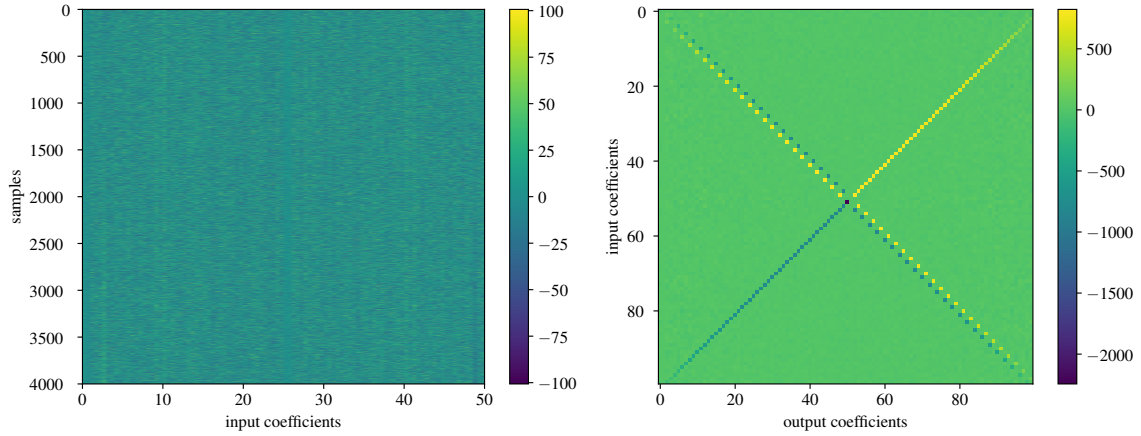

(e) Correlation image 50% noise.

(f) The p-matrix for 50% noise.

Figure 4.33: Correlation image (left column) and p-matrix (right column) for each model trained on a different noise level (row). The correlation image was sorted same order the values of the real component of wave number $k = 2$ were sorted in descending order.

The final observation we make is how for all the p-matrices the pronounced contribution of the input wave number to their corresponding output wave number. This means that the majority of contributions to each output coefficients come from the corresponding input coefficients of the same wave number. Our knowledge on how the simple derivative equation for Fourier series relate the coefficients of the derivative function and the antiderivative function aligns with the contributions shown by the p-matrices. This confirms that the model is indeed learning the relations that is defined by the derivative equation.

4.6.2 Scenario 2

The second scenario results are presented in two parts which are the coefficient predictions and function value predictions.

4.6.3 Scenario 3

CHAPTER V

SIMPULAN DAN SARAN

5.1 Simpulan

Bab ini merupakan pamungkas berupa rincian rangkuman yang merupakan simpulan dari analisis yang telah dilakukan. Simpulan ini menyajikan sejumlah hal penting yang disampaikan secara ringkas, padat, dan utuh, yang menjawab tujuan penelitian yang dituliskan pada Bab Pendahuluan. Sangat mungkin ada beberapa konsekuensi dan implikasi yang ditimbulkan dari simpulan yang dihasilkan, yang sepatutnya menjadi perhatian pada penelitian berikutnya. Judul bab dapat disesuaikan, namun umumnya ada *Simpulan* yang memang mendominasi isi bab ini.

5.2 Saran

Sejumlah ide yang muncul ketika melaksanakan penelitian TA dapat menjadi bahan atau topik untuk pekerjaan selanjutnya. Hal ini dapat berupa perbaikan atau ragam lain dari apa yang telah dilakukan sepanjang penelitian. Sub bab ini menjadi sumber informasi penting bagi, utamanya mahasiswa, yang akan melakukan penelitian lanjutan.

Bibliography

Aarts, L. P., & Van Der Veer, P. (2001). Neural Network Method for Solving Partial Differential Equations. *Neural Processing Letters*, *14*(3), 261–271. https://doi.org/10.1023/A:1012784129883

Abramowitz, M., & Stegun, I. A. (1972). *Handbook of mathematical functions: With formulas, graphs and mathematical tables [conference under the auspices of the National science foundation and the Massachussetts institute of technology]* (Unabridged, unaltered and corr. republ. of the 1964 ed). Dover publ.

Ahsan, M., Mahmud, M., Saha, P., Gupta, K., & Siddique, Z. (2021). Effect of Data Scaling Methods on Machine Learning Algorithms and Model Performance. *Technologies*, *9*(3), 52. https://doi.org/10.3390/technologies9030052

Ansel, J., Yang, E., He, H., Gimelshein, N., Jain, A., Voznesensky, M., Bao, B., Bell, P., Berard, D., Burovski, E., Chauhan, G., Chourdia, A., Constable, W., Desmaison, A., DeVito, Z., Ellison, E., Feng, W., Gong, J., Gschwind, M., … Chintala, S. (2024). PyTorch 2: Faster machine learning through dynamic python bytecode transformation and graph compilation. *29th ACM International Conference on Architectural Support for Programming Languages and Operating Systems, Volume 2 (ASPLOS '24)*. https://doi.org/10.1145/3620665.3640366

Anselmo, L., & Pardini, C. (2005). Computational methods for reentry trajectories and risk assessment. *Advances in Space Research*, *35*(7), 1343–1352. https://doi.org/10.1016/j.asr.2005.04.089

Anwar, M. R., Liu, D. L., Macadam, I., & Kelly, G. (2013). Adapting agriculture to climate change: A review. *Theoretical and Applied Climatology*, *113*(1-2), 225–245. https://doi.org/10.1007/s00704-012-0780-1

Astitha, M., & Nikolopoulos, E. (Eds.). (2023). *Extreme weather forecasting : State of the science, uncertainty and impacts*. Elsevier.
OCLC: 1347429101.

Banks, J., Hittinger, J., Connors, J., & Woodward, C. (2012). Numerical error estimation for nonlinear hyperbolic PDEs via nonlinear error transport. *Computer Methods in Applied Mechanics and Engineering*, *213–216*, 1–15. https://doi.org/10.1016/j.cma.2011.11.021

Barter, G. E. (2008). *Shock capturing with PDE-based artificial viscosity for an adaptive, higher-order discontinuous Galerkin finite element method* [Doctoral dissertation, Massachusetts Institute of Technology]. Retrieved November 9, 2024, from http://dspace.mit.edu/handle/1721.1/7582

Basir, S., & Senocak, I. (2022). Critical Investigation of Failure Modes in Physics-informed Neural Networks. *AIAA SCITECH 2022 Forum*. https://doi.org/10.2514/6.2022-2353

Bec, J., & Khanin, K. (2007). Burgers turbulence. *Physics Reports*, *447*(1-2), 1–66. https://doi.org/10.1016/j.physrep.2007.04.002

Ben-Hur, A., & Weston, J. (2010). A User's Guide to Support Vector Machines. In O. Carugo & F. Eisenhaber (Eds.), *Data Mining Techniques for the Life Sciences* (pp. 223–239, Vol. 609). Humana Press. https://doi.org/10.1007/978-1-60327-241-4_13

Benton, E. R., & Platzman, G. W. (1972). A table of solutions of the one-dimensional Burgers equation. *Quarterly of Applied Mathematics*, *30*(2), 195–212. https://doi.org/10.1090/qam/306736

Berliner, L. M. (2003). Physical-statistical modeling in geophysics. *Journal of Geophysical Research: Atmospheres*, *108*(D24), 2002JD002865. https://doi.org/10.1029/2002JD002865

Bernardi, M., Sánchez, H. D., Sheth, R. K., Brownstein, J. R., & Lane, R. R. (2022). Stellar population analysis of MaNGA early-type galaxies: IMF dependence and systematic effects. *Monthly Notices of the Royal Astronomical Society*, *518*(3), 4713–4733. https://doi.org/10.1093/mnras/stac3287

Bittner, K., & Spence, I. (2006). *Managing Iterative Software Development Projects*. Pearson Education, Limited.
OCLC: 1348491270.

Bonev, B., Kurth, T., Hundt, C., Pathak, J., Baust, M., Kashinath, K., & Anandkumar, A. (2023, July 23–29). Spherical Fourier neural operators: Learning stable dynamics on the sphere. In A. Krause, E. Brunskill, K. Cho, B. Engelhardt, S. Sabato, & J. Scarlett (Eds.), *Proceedings of the 40th international conference on machine learning* (pp. 2806–2823, Vol. 202). PMLR. https://proceedings.mlr.press/v202/bonev23a.html

Bonkile, M. P., Awasthi, A., Lakshmi, C., Mukundan, V., & Aswin, V. S. (2018). A systematic literature review of Burgers' equation with recent advances. *Pramana*, *90*(6), 69. https://doi.org/10.1007/s12043-018-1559-4

Brauer, F., Castillo-Chávez, C., & Feng, Z. (2019). *Mathematical models in epidemiology*. Springer.

Buoni, M., & Petzold, L. (2007). An efficient, scalable numerical algorithm for the simulation of electrochemical systems on irregular domains. *Journal of Computational Physics*, *225*(2), 2320–2332. https://doi.org/10.1016/j.jcp.2007.03.025

C3S. (2018). *ERA5 hourly data on single levels from 1940 to present*. https://doi.org/10.24381/CDS.ADBB2D47

Chen, J.-S., Hillman, M., & Chi, S.-W. (2017). Meshfree Methods: Progress Made after 20 Years. *Journal of Engineering Mechanics*, *143*(4), 04017001. https://doi.org/10.1061/(ASCE)EM.1943-7889.0001176

Chen, R. T. Q. (2021, June). *Torchdiffeq* (Version 0.2.2). https://github.com/rtqichen/torchdiffeq

Chen, T., & Chen, H. (1995). Universal approximation to nonlinear operators by neural networks with arbitrary activation functions and its application to dynamical systems. *IEEE Transactions on Neural Networks*, *6*(4), 911–917. https://doi.org/10.1109/72.392253

Climate change 2022: Impacts, adaptation and vulnerability : Working Group II contribution to the Sixth Assessment Report of the Intergovernmental Panel on Climate Change. (2023). Cambridge University Press.
OCLC: 1391150208.

Cogato, A., Meggio, F., De Antoni Migliorati, M., & Marinello, F. (2019). Extreme Weather Events in Agriculture: A Systematic Review. *Sustainability*, *11*(9), 2547. https://doi.org/10.3390/su11092547

Cybenko, G. (1989). Approximation by superpositions of a sigmoidal function. *Mathematics of Control, Signals, and Systems*, *2*(4), 303–314. https://doi.org/10.1007/BF02551274

Discrete Fourier Transform. (n.d.). Retrieved December 11, 2024, from https://www.mathworks.com/help/signal/ug/discrete-fourier-transform.html

Du, Y., Chalapathi, N., & Krishnapriyan, A. S. (2024). Neural spectral methods: Self-supervised learning in the spectral domain. *The Twelfth International*

Conference on Learning Representations. https://openreview.net/forum?id=2DbVeuoa6a

Eustace, S. (2024, May 8). *Poetry: Python packaging and dependency management made easy* (Version 1.8.3). Retrieved December 9, 2024, from https://python-poetry.org

Fanaskov, V. S., & Oseledets, I. V. (2023). Spectral Neural Operators. *Doklady Mathematics*, *108*(S2), S226–S232. https://doi.org/10.1134/S1064562423701107

Florêncio, A., Gabriel Rudloff, & Madson Dias. (2020, December 10). *Lssvr* (Version 0.1.0). Retrieved July 9, 2023, from https://github.com/zealberth/lssvr

Galkin, I. A., Reinisch, B. W., Vesnin, A. M., Bilitza, D., Fridman, S., Habarulema, J. B., & Veliz, O. (2020). Assimilation of sparse continuous near-earth weather measurements by NECTAR model morphing. *Space weather : the international journal of research & applications*, *18*(11), e2020SW002463. https://doi.org/10.1029/2020SW002463

Gao, H., Sun, L., & Wang, J.-X. (2021a). PhyGeoNet: Physics-informed geometry-adaptive convolutional neural networks for solving parameterized steady-state PDEs on irregular domain. *Journal of Computational Physics*, *428*, 110079. https://doi.org/10.1016/j.jcp.2020.110079

Gao, H., Sun, L., & Wang, J.-X. (2021b). Super-resolution and denoising of fluid flow using physics-informed convolutional neural networks without high-resolution labels. *Physics of Fluids*, *33*(7), 073603. https://doi.org/10.1063/5.0054312

Gaul, L., Klein, P., & Plenge, M. (1991). Simulation of wave propagation in irregular soil domains by BEM and associated small scale experiments. *Engineering Analysis with Boundary Elements*, *8*(4), 200–205. https://doi.org/10.1016/0955-7997(91)90014-K

GCSFS — GCSFs 2023.12.2post1+1.g8e500c6.dirty documentation. (n.d.). Retrieved November 26, 2024, from https://gcsfs.readthedocs.io/en/latest/

Getting Started on Kaggle | Kaggle. (n.d.). Retrieved September 9, 2024, from https://www.kaggle.com/docs/notebooks#technical-specifications

Givoni, M. (2006). Development and Impact of the Modern High-speed Train: A Review. *Transport Reviews*, *26*(5), 593–611. https://doi.org/10.1080/01441640600589319

Gong, X., Herty, M., Piccoli, B., & Visconti, G. (2023). Crowd Dynamics: Modeling and Control of Multiagent Systems. *Annual Review of Control, Robotics, and Autonomous Systems*, *6*(1), 261–282. https://doi.org/10.1146/annurev-control-060822-123629

Govind, R., Garg, N., & Mittal, V. (2020). Weather, Affect, and Preference for Hedonic Products: The Moderating Role of Gender. *Journal of Marketing Research*, *57*(4), 717–738. https://doi.org/10.1177/0022243720925764

Haifeng Wang & Dejin Hu. (2005). Comparison of SVM and LS-SVM for Regression. *2005 International Conference on Neural Networks and Brain*, *1*, 279–283. https://doi.org/10.1109/ICNNB.2005.1614615

Herrera, M., Natarajan, S., Coley, D. A., Kershaw, T., Ramallo-González, A. P., Eames, M., Fosas, D., & Wood, M. (2017). A review of current and future weather data for building simulation. *Building Services Engineering Research and Technology*, *38*(5), 602–627. https://doi.org/10.1177/0143624417705937

Holmes, E. E., Lewis, M. A., Banks, J. E., & Veit, R. R. (1994). Partial Differential Equations in Ecology: Spatial Interactions and Population Dynamics. *Ecology*, *75*(1), 17–29. https://doi.org/10.2307/1939378

Hornik, K., Stinchcombe, M., & White, H. (1989). Multilayer feedforward networks are universal approximators. *Neural Networks*, *2*(5), 359–366. https://doi.org/10.1016/0893-6080(89)90020-8

Hoyer, S., & Hamman, J. (2017). Xarray: N-D labeled arrays and datasets in Python. *Journal of Open Research Software*, *5*(1). https://doi.org/10.5334/jors.148

Hoyer, S., Roos, M., Joseph, H., Magin, J., Cherian, D., Fitzgerald, C., Hauser, M., Fujii, K., Maussion, F., Imperiale, G., Clark, S., Kleeman, A., Nicholas, T., Kluyver, T., Westling, J., Munroe, J., Amici, A., Barghini, A., Banihirwe, A., … Littlejohns, O. (2024, September 11). *Xarray* (Version v2024.09.0). https://doi.org/10.5281/ZENODO.13750907

Hughes, R. (2000). The flow of large crowds of pedestrians. *Mathematics and Computers in Simulation*, *53*(4-6), 367–370. https://doi.org/10.1016/S0378-4754(00)00228-7

Jameson, A. (2007). Energy Estimates for Nonlinear Conservation Laws with Applications to Solutions of the Burgers Equation and One-Dimensional Vicous Flow in a Shock Tube by Central Difference Schemes. *18th AIAA*

Computational Fluid Dynamics Conference. https://doi.org/10.2514/6.2007-4620

Jia, Y., Liu, K., & Zhang, X. S. (2024). Modulate stress distribution with bio-inspired irregular architected materials towards optimal tissue support. *Nature Communications*, *15*(1), 4072. https://doi.org/10.1038/s41467-024-47831-2

Jin, M., Wang, L., Ge, F., & Yan, J. (2023). Detecting the interaction between urban elements evolution with population dynamics model. *Scientific Reports*, *13*(1), 12367. https://doi.org/10.1038/s41598-023-38979-w

Kapoor, S., & Narayanan, A. (2023). Leakage and the reproducibility crisis in machine-learning-based science. *Patterns*, *4*(9), 100804. https://doi.org/10.1016/j.patter.2023.100804

Kaufman, S., Rosset, S., Perlich, C., & Stitelman, O. (2012). Leakage in data mining: Formulation, detection, and avoidance. *ACM Transactions on Knowledge Discovery from Data*, *6*(4), 1–21. https://doi.org/10.1145/2382577.2382579

Krishnapriyan, A., Gholami, A., Zhe, S., Kirby, R., & Mahoney, M. W. (2021). Characterizing possible failure modes in physics-informed neural networks. In M. Ranzato, A. Beygelzimer, Y. Dauphin, P. Liang, & J. W. Vaughan (Eds.), *Advances in neural information processing systems* (pp. 26548–26560, Vol. 34). Curran Associates, Inc. https://proceedings.neurips.cc/paper_files/paper/2021/file/df438e5206f31600e6ae4af72f2725f1-Paper.pdf

Kurth, T., Subramanian, S., Harrington, P., Pathak, J., Mardani, M., Hall, D., Miele, A., Kashinath, K., & Anandkumar, A. (2023). FourCastNet: Accelerating Global High-Resolution Weather Forecasting Using Adaptive Fourier Neural Operators. *Proceedings of the Platform for Advanced Scientific Computing Conference*, 1–11. https://doi.org/10.1145/3592979.3593412

Kwasniok, F. (2012). Data-based stochastic subgrid-scale parametrization: An approach using cluster-weighted modelling. *Philosophical Transactions of the Royal Society A: Mathematical, Physical and Engineering Sciences*, *370*(1962), 1061–1086. https://doi.org/10.1098/rsta.2011.0384

Larios, A. (2021, April 28). *MATH 934 – BURGERS EQUATION PROJECT* [handout]. Retrieved September 16, 2024, from https://www.math.unl.edu/~alarios2/courses/2017_spring_M934/documents/burgersProject.pdf

Leake, C., Johnston, H., Smith, L., & Mortari, D. (2019). Analytically Embedding Differential Equation Constraints into Least Squares Support Vector Machines Using the Theory of Functional Connections. *Machine Learning and Knowledge Extraction*, *1*(4), 1058–1083. https://doi.org/10.3390/make1040060

Lepage, S., & Morency, C. (2021). Impact of Weather, Activities, and Service Disruptions on Transportation Demand. *Transportation Research Record: Journal of the Transportation Research Board*, *2675*(1), 294–304. https://doi.org/10.1177/0361198120966326

Li, Z., Kovachki, N. B., Azizzadenesheli, K., liu, B., Bhattacharya, K., Stuart, A., & Anandkumar, A. (2021). Fourier neural operator for parametric partial differential equations. *International Conference on Learning Representations*. https://openreview.net/forum?id=c8P9NQVtmnO

Lu, L., Jin, P., Pang, G., Zhang, Z., & Karniadakis, G. E. (2021). Learning nonlinear operators via DeepONet based on the universal approximation theorem of operators. *Nature Machine Intelligence*, *3*(3), 218–229. https://doi.org/10.1038/s42256-021-00302-5

Malhi, G. S., Kaur, M., & Kaushik, P. (2021). Impact of Climate Change on Agriculture and Its Mitigation Strategies: A Review. *Sustainability*, *13*(3), 1318. https://doi.org/10.3390/su13031318

Mehrkanoon, S., & Suykens, J. A. (2015). Learning solutions to partial differential equations using LS-SVM. *Neurocomputing*, *159*, 105–116. https://doi.org/10.1016/j.neucom.2015.02.013

Mengaldo, G., Wyszogrodzki, A., Diamantakis, M., Lock, S.-J., Giraldo, F. X., & Wedi, N. P. (2019). Current and Emerging Time-Integration Strategies in Global Numerical Weather and Climate Prediction. *Archives of Computational Methods in Engineering*, *26*(3), 663–684. https://doi.org/10.1007/s11831-018-9261-8

Monmonier, M. S. (1999). *Air apparent: How meteorologists learned to map, predict, and dramatize weather*. Univ. of Chicago Press.

Moon, S., Kang, M. Y., Bae, Y. H., & Bodkin, C. D. (2018). Weather sensitivity analysis on grocery shopping. *International Journal of Market Research*, *60*(4), 380–393. https://doi.org/10.1177/1470785317751614

Mukherjee, S., Goswami, D., & Chatterjee, S. (2015). A Lagrangian Approach to Modeling and Analysis of a Crowd Dynamics. *IEEE Transactions on Systems,*

Man, and Cybernetics: Systems, *45*(6), 865–876. https://doi.org/10.1109/TSMC.2015.2389763

Muller, A. P. O., Costa, J. C., Bom, C. R., Klatt, M., Faria, E. L., de Albuquerque, M. P., & de Albuquerque, M. P. (2023). Deep pre-trained FWI: Where supervised learning meets the physics-informed neural networks. *Geophysical Journal International*, *235*(1), 119–134. https://doi.org/10.1093/gji/ggad215

Nash, C. (1991, January). *The case for high speed rail* (Working Paper No. Working Paper 323). Institute of Transport Studies, University of Leeds / ARRAY(0x5581272c4498). Leeds, UK. https://eprints.whiterose.ac.uk/2236/

Ni, P., Sun, L., Yang, J., & Li, Y. (2022). Multi-End Physics-Informed Deep Learning for Seismic Response Estimation. *Sensors*, *22*(10), 3697. https://doi.org/10.3390/s22103697

Nurmi, P., Perrels, A., & Nurmi, V. (2013). Expected impacts and value of improvements in weather forecasting on the road transport sector. *Meteorological Applications*, *20*(2), 217–223. https://doi.org/10.1002/met.1399

Orlandi, P. (2000). The Burgers equation. In P. Orlandi (Ed.). R. Moreau (**typeredactor**), *Fluid Flow Phenomena* (pp. 40–50, Vol. 55). Springer Netherlands. https://doi.org/10.1007/978-94-011-4281-6_4

Orszag, S. A. (1971). On the Elimination of Aliasing in Finite-Difference Schemes by Filtering High-Wavenumber Components. *Journal of the Atmospheric Sciences*, *28*(6), 1074–1074. https://doi.org/10.1175/1520-0469(1971)028<1074:OTEOAI>2.0.CO;2

Orszag, S. A. (1972). Comparison of Pseudospectral and Spectral Approximation. *Studies in Applied Mathematics*, *51*(3), 253–259. https://doi.org/10.1002/sapm1972513253

Preston-Werner, T. (n.d.). *Semantic Versioning 2.0.0*. Semantic Versioning. Retrieved September 9, 2024, from https://semver.org/

Raissi, M., Perdikaris, P., & Karniadakis, G. (2019). Physics-informed neural networks: A deep learning framework for solving forward and inverse problems involving nonlinear partial differential equations. *Journal of Computational Physics*, *378*, 686–707. https://doi.org/10.1016/j.jcp.2018.10.045

Rasp, S., Hoyer, S., Merose, A., Langmore, I., Battaglia, P., Russel, T., Sanchez-Gonzalez, A., Yang, V., Carver, R., Agrawal, S., Chantry, M., Bouallegue, Z. B., Dueben, P., Bromberg, C., Sisk, J., Barrington, L., Bell, A.,

& Sha, F. (2023). WeatherBench 2: A benchmark for the next generation of data-driven global weather models.

Rathore, P., Lei, W., Frangella, Z., Lu, L., & Udell, M. (2024). *Challenges in Training PINNs: A Loss Landscape Perspective* (2). https://doi.org/10.48550/ARXIV.2402.01868

Reinhardt, J. C., Chen, X., Liu, W., Manchev, P., & Paté-Cornell, M. E. (2016). Asteroid Risk Assessment: A Probabilistic Approach. *Risk Analysis*, *36*(2), 244–261. https://doi.org/10.1111/risa.12453

Roberts, M., & Bowman, J. C. (2011). Dealiased convolutions for pseudospectral simulations. *Journal of Physics: Conference Series*, *318*(7), 072037. https://doi.org/10.1088/1742-6596/318/7/072037

Sadiku, M. N. O., & Obiozor, C. N. (2000). A Simple Introduction to the Method of Lines. *International Journal of Electrical Engineering & Education*, *37*(3), 282–296. https://doi.org/10.7227/IJEEE.37.3.8

Schiesser, W. E. (2012). *The Numerical Method of Lines: Integration of Partial Differential Equations*. Elsevier Science.

Shen, J. (2011). *Spectral Methods: Algorithms, Analysis and Applications*. Springer. https://doi.org/10.1007/978-3-540-71041-7

Shrestha, A., & Mahmood, A. (2019). Review of Deep Learning Algorithms and Architectures. *IEEE Access*, *7*, 53040–53065. https://doi.org/10.1109/ACCESS.2019.2912200

Soydaner, D. (2020). A Comparison of Optimization Algorithms for Deep Learning. *International Journal of Pattern Recognition and Artificial Intelligence*, *34*(13), 2052013. https://doi.org/10.1142/S0218001420520138

Spanos, A. (2006). Where do statistical models come from? Revisiting the problem of specification. In *Institute of Mathematical Statistics Lecture Notes - Monograph Series* (pp. 98–119). Institute of Mathematical Statistics. https://doi.org/10.1214/074921706000000419

Stott, P. A., Christidis, N., Otto, F. E. L., Sun, Y., Vanderlinden, J.-P., van Oldenborgh, G. J., Vautard, R., von Storch, H., Walton, P., Yiou, P., & Zwiers, F. W. (2016). Attribution of extreme weather and climate-related events. *WIREs Climate Change*, *7*(1), 23–41. https://doi.org/10.1002/wcc.380

Suykens, J. A. K. (Ed.). (2005). *Least squares support vector machines* (Repr). World Scientific.

Tabatabaei, A. H. A., Shakour, E., & Dehghan, M. (2007). Some implicit methods for the numerical solution of Burgers' equation. *Applied Mathematics and Computation*, *191*(2), 560–570. https://doi.org/10.1016/j.amc.2007.02.158

Tian, J., Zhang, Y., & Zhang, C. (2018). Predicting consumer variety-seeking through weather data analytics. *Electronic Commerce Research and Applications*, *28*, 194–207. https://doi.org/10.1016/j.elerap.2018.02.001

Tian, X., Cao, S., & Song, Y. (2021). The impact of weather on consumer behavior and retail performance: Evidence from a convenience store chain in China. *Journal of Retailing and Consumer Services*, *62*, 102583. https://doi.org/10.1016/j.jretconser.2021.102583

Turchin, P. (2001). Does population ecology have general laws? *Oikos*, *94*(1), 17–26. https://doi.org/10.1034/j.1600-0706.2001.11310.x

Üstün, B., Melssen, W., & Buydens, L. (2007). Visualisation and interpretation of Support Vector Regression models. *Analytica Chimica Acta*, *595*(1-2), 299–309. https://doi.org/10.1016/j.aca.2007.03.023

Uzan, J.-P. (2003). The fundamental constants and their variation: Observational and theoretical status. *Reviews of Modern Physics*, *75*(2), 403–455. https://doi.org/10.1103/RevModPhys.75.403

Vapnik, V. N. (2000). *The Nature of Statistical Learning Theory* (2nd ed). Springer New York. https://doi.org/10.1007/978-1-4757-3264-1

Wang, R., Kashinath, K., Mustafa, M., Albert, A., & Yu, R. (2020). Towards Physics-informed Deep Learning for Turbulent Flow Prediction. *Proceedings of the 26th ACM SIGKDD International Conference on Knowledge Discovery & Data Mining*, 1457–1466. https://doi.org/10.1145/3394486.3403198

Wang, X., & Zhang, W. (2019). Efficiency and Spatial Equity Impacts of High-Speed Rail on the Central Plains Economic Region of China. *Sustainability*, *11*(9), 2583. https://doi.org/10.3390/su11092583

Wazwaz, A.-M. (2010). *Partial Differential Equations and Solitary Waves Theory*. Springer Berlin Heidelberg. https://doi.org/10.1007/978-3-642-00251-9

Wilby, R. L., & Yu, D. (2013). Rainfall and temperature estimation for a data sparse region. *Hydrology and Earth System Sciences*, *17*(10), 3937–3955. https://doi.org/10.5194/hess-17-3937-2013

Wood, W. L. (2006). An exact solution for Burger's equation. *Communications in Numerical Methods in Engineering*, *22*(7), 797–798. https://doi.org/10.1002/cnm.850

Youxi Wu, Ying Li, Lei Guo, Weili Yan, Xueqin Shen, & Kun Fu. (2005). SVM for Solving Forward Problems of EIT. *2005 IEEE Engineering in Medicine and Biology 27th Annual Conference*, 1559–1562. https://doi.org/10.1109/IEMBS.2005.1616732

Zhang, R., Liu, Y., & Sun, H. (2020). Physics-guided convolutional neural network (PhyCNN) for data-driven seismic response modeling. *Engineering Structures*, *215*, 110704. https://doi.org/10.1016/j.engstruct.2020.110704

Zhao, X., Gong, Z., Zhang, Y., Yao, W., & Chen, X. (2023). Physics-informed convolutional neural networks for temperature field prediction of heat source layout without labeled data. *Engineering Applications of Artificial Intelligence*, *117*, 105516. https://doi.org/10.1016/j.engappai.2022.105516

APPENDIX A

KODE PROGRAM

1.1 PROGRAM SATU

1.2 PROGRAM DUA

APPENDIX B

GAMBAR-GAMBAR